Research Article

Local Strain Rate and Curvature Dependences of Scalar Dissipation Rate Transport in Turbulent Premixed Flames: A Direct Numerical Simulation Analysis

Y. Gao,[1] N. Chakraborty,[1] and N. Swaminathan[2]

[1] *School of Mechanical and Systems Engineering, Newcastle University, Claremont Road, Newcastle-Upon-Tyne NE1 7RU, UK*
[2] *Cambridge University Engineering Department, Trumpington Street, Cambridge CB2 1PZ, UK*

Correspondence should be addressed to N. Chakraborty; nilanjan.chakraborty@newcastle.ac.uk

Received 5 December 2013; Accepted 31 January 2014 Published 3 April 2014

Academic Editor: Michael Fairweather

The statistical behaviours of the instantaneous scalar dissipation rate N_c of reaction progress variable c in turbulent premixed flames have been analysed based on three-dimensional direct numerical simulation data of freely propagating statistically planar flame and V-flame configurations with different turbulent Reynolds number Re_t. The statistical behaviours of N_c and different terms of its transport equation for planar and V-flames are found to be qualitatively similar. The mean contribution of the density-variation term T_1 is positive, whereas the molecular dissipation term $(-D_2)$ acts as a leading order sink. The mean contribution of the strain rate term T_2 is predominantly negative for the cases considered here. The mean reaction rate contribution T_3 is positive (negative) towards the unburned (burned) gas side of the flame, whereas the mean contribution of the diffusivity gradient term (D) assumes negative (positive) values towards the unburned (burned) gas side. The local statistical behaviours of N_c, T_1, T_2, T_3, $(-D_2)$, and $f(D)$ have been analysed in terms of their marginal probability density functions (pdfs) and their joint pdfs with local tangential strain rate a_T and curvature k_m. Detailed physical explanations have been provided for the observed behaviour.

1. Introduction

Scalar dissipation rate (SDR) plays a pivotal role in turbulent reacting flows [1, 2] and thus its statistical behaviour is of fundamental importance to the modelling of turbulent premixed combustion. In turbulent premixed combustion the mean/filtered reaction rate $\overline{\dot{w}}$ of a reaction progress variable c is directly related to the Favre mean/filtered value of SDR $\widetilde{N}_c = \overline{\rho D \nabla c \cdot \nabla c}/\overline{\rho}$ [1–4], where ρ is the fluid density and D is the progress variable diffusivity with the overbar indicating a Reynolds averaging/large eddy simulation (LES) filtering process as applicable. It is well known that strain rate and curvature can significantly affect the local flame propagation behaviour and $|\nabla c|$ statistics in turbulent premixed flames [5–16]. Thus, strain rate and curvature are expected to have appreciable influences on local statistics of SDR N_c and its transport. The transport equation of the instantaneous SDR of reaction progress variable N_c is given as [3, 17]

$$\begin{aligned}
&\frac{\partial\left(\rho N_c\right)}{\partial t} + \frac{\partial\left(\rho u_j N_c\right)}{\partial x_j} \\
&\quad = \frac{\partial}{\partial x_j}\left(\rho D \frac{\partial N_c}{\partial x_j}\right) - \frac{2D}{\rho}\frac{\partial \rho}{\partial x_j}\frac{\partial c}{\partial x_j}\left[\dot{w} + \nabla\cdot\left(\rho D \nabla c\right)\right] \\
&\qquad - 2\rho D \frac{\partial c}{\partial x_i}\frac{\partial u_i}{\partial x_j}\frac{\partial c}{\partial x_j} + 2D\frac{\partial \dot{w}}{\partial x_j}\frac{\partial c}{\partial x_j} \\
&\qquad - 2\rho D^2 \frac{\partial^2 c}{\partial x_i \partial x_j}\frac{\partial^2 c}{\partial x_i \partial x_j} + f\left(D\right),
\end{aligned} \tag{1a}$$

where

$$f(D) = \underbrace{2D\frac{\partial c}{\partial x_k}\frac{\partial(\rho D)}{\partial x_k}\frac{\partial^2 c}{\partial x_j \partial x_j}}_{T_{D1}} + \underbrace{2D\frac{\partial c}{\partial x_k}\frac{\partial^2(\rho D)}{\partial x_j \partial x_k}\frac{\partial c}{\partial x_j}}_{T_{D2}} \underbrace{-\frac{\partial}{\partial x_j}\left(\rho N_c \frac{\partial D}{\partial x_j}\right)}_{T_{D3}} \underbrace{-2\rho D\frac{\partial D}{\partial x_j}\frac{\partial(\nabla c \cdot \nabla c)}{\partial x_j}}_{T_{D4}} + \underbrace{\rho \nabla c \cdot \nabla c\left[\frac{\partial D}{\partial t} + u_j \frac{\partial D}{\partial x_j}\right]}_{T_{D5}}. \quad (1b)$$

The first two terms on the left hand side of (1a) represent the transient and advection effects, whereas the first term on the right hand side (i.e., $D_1 = \nabla\cdot(\rho D \nabla N_c)$) denotes molecular diffusion of SDR. The second term on the right hand side of (1a) (i.e., $T_1 = -2D\nabla\rho \cdot \nabla c[\dot{w} + \nabla \cdot (\rho D \nabla c)]/\rho$) originates due to density variation and will henceforth be referred to as the density variation term. The third term on the right hand side of (1a) (i.e., $T_2 = -2\rho D(\partial c/\partial x_i)(\partial u_i/\partial x_j)(\partial c/\partial x_j)$) represents the effects of fluid-dynamic straining, whereas the fourth term (i.e., $T_3 = 2D(\partial \dot{w}/\partial x_i)(\partial c/\partial x_i)$) denotes the reaction rate contribution to the SDR transport. The penultimate term on the right hand side of (1a) (i.e., $-D_2 = -2\rho D^2(\partial^2 c/\partial x_i \partial x_j)(\partial^2 c/\partial x_i \partial x_j)$) denotes molecular dissipation of N_c, and the terms involving temporal and spatial gradients of diffusivity are collectively referred to as $f(D)$ (see (1b)).

Although the statistical behaviours of $|\nabla c|$ and the terms of its transport equation were analysed earlier, the terms of N_c transport equation are fundamentally different from the terms of the $|\nabla c|$ transport equation, which can be written for a given c isosurface in the following manner [11, 13–16]:

$$\frac{\partial |\nabla c|}{\partial t} + \frac{\partial\left(u_j |\nabla c|\right)}{\partial x_j} = \left(\delta_{ij} - n_i n_j\right)\frac{\partial u_i}{\partial x_j}|\nabla c| + S_d \frac{\partial n_i}{\partial x_i} - \frac{\partial\left(S_d n_i |\nabla c|\right)}{\partial x_i}, \quad (2)$$

where $n_i = -(\partial c/\partial x_i)/|\nabla c|$ is the ith component of flame normal vector and $S_d = (\dot{w} + \nabla \cdot (\rho D \nabla c))/\rho|\nabla c|$ is the local flame displacement speed. It is evident from (1a) and (1b) and (2) that the statistical behaviour of N_c transport is likely to be different from $|\nabla c|$ transport although the quantities N_c and $|\nabla c|$ are closely related to each other (i.e., $N_c = D|\nabla c|^2$).

It is often necessary to solve a transport equation for $\widetilde{N}_c$ in the context of Reynolds averaged Navier-Stokes (RANS) simulations and LES [17–30]. The transport equation for $\widetilde{N}_c$ can be obtained by Reynolds averaging or LES filtering of (1a) and (1b) as

$$\frac{\partial\left(\overline{\rho}\widetilde{N}_c\right)}{\partial t} + \frac{\partial\left(\overline{\rho}\widetilde{u}_j\widetilde{N}_c\right)}{\partial x_j} = \overline{\frac{\partial}{\partial x_j}\left(\rho D\frac{\partial N_c}{\partial x_j}\right)} - \frac{\partial\left[\overline{\rho u_i N_c} - \overline{\rho}\widetilde{u}_i\widetilde{N}_c\right]}{\partial x_i} + \overline{T}_1 + \overline{T}_2 + \overline{T}_3 - \overline{D}_2 + \overline{f(D)}. \quad (3)$$

The terms $\overline{T}_1$, $\overline{T}_2$, $\overline{T}_3$, $(-\overline{D}_2)$, and $\overline{f(D)}$ are unclosed and therefore it is important to understand the statistical behaviours of N_c, T_1, T_2, T_3, $(-D_2)$, and $f(D)$ (since $\lim_{\Delta\to 0}\widetilde{N}_c = N_c$, $\lim_{\Delta\to 0}\overline{T}_1 = T_1$, $\lim_{\Delta\to 0}\overline{T}_2 = T_2$, $\lim_{\Delta\to 0}\overline{T}_3 = T_3$, $\lim_{\Delta\to 0}(-\overline{D}_2) = (-D_2)$, and $\lim_{\Delta\to 0}\overline{f(D)} = f(D)$, where Δ is the LES filter width) and their local strain rate and curvature dependences in order to model these quantities in the context of LES, where the local strain rate and curvature dependences of these terms need to be adequately captured. The local strain rate and curvature dependences of N_c and the terms of its transport equation (i.e., T_1, T_2, T_3, and $(-D_2)$) are yet to be analysed in detail in the existing literature. This paper aims to address this gap by analysing local tangential strain rate $a_T = (\delta_{ij} - n_i n_j)\partial u_i/\partial x_j$ and curvature $\kappa_m = 0.5(\partial n_i/\partial x_i)$ (for the above definition of κ_m, the flame elements convex towards the reactants has a positive curvature) dependences of N_c, T_1, T_2, T_3, $(-D_2)$, and $f(D)$ at different locations within the flame using direct numerical simulations (DNS) data of turbulent premixed freely propagating statistically planar flame and turbulent V-flame configurations. In this respect, the main objectives of this study are as follows:

(1) to analyse local statistical behaviours of instantaneous SDR (i.e., N_c) and the terms of its transport equation T_1, T_2, T_3, $(-D_2)$, and $f(D)$;

(2) to explain the observed strain rate and curvature dependences of N_c, T_1, T_2, T_3, $(-D_2)$, and $f(D)$;

(3) to compare the statistical behaviours of instantaneous SDR and the terms of its transport equation obtained from DNS in a canonical configuration with constant thermophysical properties with DNS of a laboratory configuration (e.g., turbulent V-flame configuration) with temperature-dependent thermophysical properties.

The rest of the paper will be organised as follows. The necessary mathematical modelling and the information related to the numerical implementation of DNS simulations will be presented in the next section. This will be followed by the presentation of the results and the subsequent discussion. The main findings will be summarised and conclusions will be drawn in the final section of this paper.

2. Mathematical Background and Numerical Implementation

DNS simulations of turbulent reacting flows should address both the three-dimensionality of turbulence and detailed chemical structure of the flames. However, limitation of computer hardware until recently restricted DNS of turbulent reacting flows either to two dimensions with detailed chemistry or to three dimensions with simplified chemistry. Although it is now possible to carry out three-dimensional DNS simulations with detailed chemistry, they remain extremely expensive [31] and are often not suitable for a detailed parametric analysis especially for simulations in relatively complex configurations (e.g., V-flame). Here, three-dimensional simulations with single step Arrhenius type chemistry have been considered for an extensive parametric analysis. The parametric analysis based on freely propagating statistically planar flames in a canonical configuration has been carried out using a well-proven compressible DNS code SENGA [32]. In the context of simple chemistry, the species field is uniquely represented by a reaction progress variable c, which can be defined in terms of a suitable reactant (product) mass fraction $Y_R(Y_P)$ as $c = (Y_{R0} - Y_R)/(Y_{R0} - Y_{R\infty})(c = (Y_P - Y_{P0})/(Y_{P\infty} - Y_{P0})$, where the subscripts 0 and ∞ are used to denote the values in unburned reactants and fully burned products, respectively. For the simulations of freely propagating statistically planar flames (i.e., cases P1–P5, where "P" denotes the statistically planar flames), a rectangular domain of size $36.1\delta_{\text{th}} \times 24.1\delta_{\text{th}} \times 24\delta_{\text{th}}$ is considered, where $\delta_{\text{th}} = (T_{\text{ad}} - T_0)/\operatorname{Max}|\nabla\widehat{T}|_L$ is the thermal flame thickness with T_{ad}, T_0, and $\widehat{T}$ being the adiabatic flame, unburned reactant, and instantaneous dimensional temperatures, respectively, and the subscript "L" refers to the unstrained laminar flame quantities. For the thermochemistry used in cases P1–P5, the thermal flame thickness δ_{th} is found to be $1.785D_0/S_L$ (i.e., $\delta_{\text{th}} = 1.785D_0/S_L$), where D_0 is the mass diffusivity in the unburned gas.

The simulation domain for cases P1–P5 is discretised using a uniform Cartesian grid of $345 \times 230 \times 230$. The largest side of the domain is taken to align with the mean direction of flame propagation and the boundaries in that direction are taken to be partially nonreflecting. The partially nonreflecting boundary conditions are specified using the Navier-Stokes characteristic boundary conditions (NSCBC) technique [33]. The transverse directions are taken to be periodic and thus do not need any separate boundary conditions. A 10th order central-difference scheme is used to evaluate spatial derivatives at the internal grid points but the order of differentiation gradually drops to a one-sided 4th order scheme near nonperiodic boundaries. The time-advancement is carried out using a 3rd order low storage Runge-Kutta scheme [34]. One does not obtain any spurious fluctuations due to the 10th order central difference scheme and its transition to the lower-order finite difference scheme for sufficiently small grid spacing (e.g., $\Delta x \leq \eta$, where Δx and η are the grid spacing and the Kolmogorov length scale, respectively). Thus it was not necessary to use numerical filter to eliminate spurious oscillations. The flames in cases P1–P5 remain sufficiently away from the domain boundaries whereas the major part of the reactive region in cases V1–V3 does not interact with the nonperiodic boundaries except for flame crossing the outlet boundary. For the present analysis, the regions of flame crossing nonperiodic boundary are not considered for extracting SDR statistics in cases V1–V3. Thus, the evaluation of SDR and the terms of its transport equation at a given point of time is nominally 10th order accurate in this analysis. It is worth noting that similar numerical schemes for spatial discretisation and time advancement were used in several previous studies [4–17, 22–32].

The initial values of root-mean-square turbulent velocity fluctuation normalised by unstrained laminar burning velocity u'/S_L, integral length scale to flame thickness ratio l/δ_{th}, turbulent Reynolds number $\text{Re}_t = \rho_0 u' l/\mu_0$, Damköhler number $\text{Da} = lS_L/u'\delta_{\text{th}}$ and Karlovitz number $\text{Ka} = (u'/S_L)^{3/2}(l/\delta_{\text{th}})^{-1/2}$, heat release parameter $\tau = (T_{\text{ad}} - T_0)/T_0$, and Zel'dovich number $\beta = T_{\text{ac}}(T_{\text{ad}} - T_0)/T_{\text{ad}}^2$ for cases P1–P5 are provided in Table 1, where ρ_0 and μ_0 are the unburned gas density and viscosity, respectively, and T_{ac} is the activation temperature. As Re_t scales as $\text{Re}_t \sim \text{Da}^2\text{Ka}^2$ [35], the change in turbulent Reynolds number in cases P1–P5 is brought about by modifying Da and Ka independently of each other (e.g., Da (Ka) is kept unaltered in cases P1, P3, and P5 (P2, P3, and P4)). In cases P1–P5, the flame-turbulence interaction takes place under decaying turbulence, which necessitates a simulation time $t_{\text{sim}} \geq \operatorname{Max}(t_f, t_c)$, where $t_f = l/u'$ is the initial eddy turn over time and $t_c = \delta_{\text{th}}/S_L$ is the chemical time scale. In all cases, statistics were extracted after one chemical time scale t_c, which corresponds to a time equal to $2.0t_f$ in case P4, $3.0t_f$ in cases P1, P3, and P5, and $4.34t_f$ for case P2. It is worth noting that the chemical time scale t_c remains the same for all cases due to identical thermochemistry. The present simulation time is comparable to the simulation times used for several previous DNS studies [5–9, 12, 36–39]. The global level of turbulent velocity fluctuation had decayed by 52.66%, 61.11%, 45%, 24%, and 34% in comparison to the initial values for cases P1–P5, respectively. By contrast, the integral length scale increased by factors between 1.5 and 2.25, ensuring that sufficient numbers of turbulent eddies were retained in each direction to obtain useful statistics. The values for u'/S_L, l/δ_{th}, and δ_{th}/η at the time when statistics were extracted have been presented elsewhere [39] and thus are not repeated here. For cases P1–P5, the thermal flame thickness δ_{th} is greater than the Kolmogorov length scale η at the time of the analysis, and this suggests that combustion in these cases takes place in the thin reaction zones regime [35]. The temporal evolutions of turbulent kinetic energy evaluated over the whole domain and the global burning rate were shown in [39], which demonstrate that these quantities were not varying rapidly with time when the statistics were extracted. It was also shown in [39] that the flame propagation statistics remain unchanged halfway through the simulation.

The V-flame cases (i.e., cases V1, V2, and V3, where "V" denotes V-shape flames here) are simulated using an updated version of SENGA and SENGA2 [40, 41] with ability to handle complex chemistry. However, the V-flames were simulated

Table 1: Initial values of simulation parameters and nondimensional numbers relevant to the DNS database considered here.

Case	Domain size/δ_{th}^3	Grid size	u'/S_L	l/δ_{th}	τ	Re_t	Da	Ka	β
P1	$36.1 \times 24.1 \times 24.1$	$345 \times 230 \times 230$	5.0	1.67	4.5	22.0	0.33	8.67	6.0
P2	$36.1 \times 24.1 \times 24.1$	$345 \times 230 \times 230$	6.25	1.44	4.5	23.5	0.23	13.0	6.0
P3	$36.1 \times 24.1 \times 24.1$	$345 \times 230 \times 230$	7.5	2.50	4.5	48.0	0.33	13.0	6.0
P4	$36.1 \times 24.1 \times 24.1$	$345 \times 230 \times 230$	9.0	4.31	4.5	100	0.48	13.0	6.0
P5	$36.1 \times 24.1 \times 24.1$	$345 \times 230 \times 230$	11.25	3.75	4.5	110	0.33	19.5	6.0
V1	$29.7 \times 29.7 \times 29.7$	$512 \times 512 \times 512$	1.0	3.57	2.52	18	3.59	0.529	7.1
V2	$29.7 \times 29.7 \times 29.7$	$512 \times 512 \times 512$	2.0	3.62	2.52	37	1.81	1.487	7.1
V3	$29.7 \times 29.7 \times 29.7$	$512 \times 512 \times 512$	6.0	3.43	2.52	92	0.57	7.936	7.1

using a single step chemistry to keep the comparison with statistically planar flames consistent. All the nonperiodic boundaries are specified using the NSCBC technique [33]. Nonreflecting outflows, modified to accommodate the presence of flame on the boundary, were applied to the transverse and downstream faces [40, 41]. Inlet turbulence was taken from a precomputed simulation of fully developed homogeneous isotropic turbulence, and the velocity components were interpolated onto the inlet using a high-order scheme to ensure that the structure of the turbulence was preserved. The computational domain in cases V1–V3 is taken to be cubic with sides equal to $L = 29.7\delta_{th}$, where $\delta_{th} = 3.563D_0/S_L$ for the thermochemistry used in these cases. A Cartesian grid of $512 \times 512 \times 512$ with uniform grid spacing is used. The numerical schemes used for spatial discretisation and time-integration in cases V1–V3 are similar to those used for cases P1–P5. The flame holder centre is located at $x_1 = 3.48\delta_{th}$ and has an approximate radius $R = 1.2\delta_{th}$. At the flame holder, the reaction progress variable and mean velocity distributions were imposed using a Gaussian function. It is worth noting that formation of boundary layer around the flame holder and its effect on the flow and flame dynamics are not represented in the simulation due to prohibitive computational cost. However, the possible influence of these effects on the results reported in this study is minimised by carefully selecting the region for the analysis. In the selected regions, the statistical distributions of strain and curvature experienced by flame elements are similar to those for freely propagating statistically planar flames under comparable local conditions [40, 41]. The values of turbulent Reynolds number $Re_{t,inlet} = \rho_0 u'_{inlet} l/\mu_0$, Karlovitz number $Ka = (u'_{inlet}/S_L)^{3/2}(l/\delta_{th})^{-1/2}$, and Damköhler number $Da = lS_L/u'_{inlet}\delta_{th}$ based on the root-mean-square turbulent velocity fluctuation u'_{inlet} at the inlet are provided in Table 1 along with the values of τ and β.

To ensure that initial transients had decayed and a stationary state had been reached, the simulation was carried out for a period of one flow-through time $\tau_{FT} = L/\overline{U}_{in}$ before data were collected for analysis, where $\overline{U}_{in}$ is the mean inlet velocity. In the V-flame configuration, the flame is continuously developing downstream from the flame holder, and so the present analysis is restricted to a region spanning $14.9\delta_{th} \le x_1 \le 29.1\delta_{th}$ in the streamwise direction, thus ensuring sufficient time for the flame to develop following ignition. For the purpose of ensuring adequate convergence of the statistics, four snapshots from the simulation were used to obtain SDR statistics presented in the next section, which are taken at an interval of $0.2\tau_{FT}$ after the initial flow-through time. Standard values have been taken for Prandtl number (Pr = 0.7) and ratio of specific heats, $\gamma = 1.4$. The global Lewis number is taken to be unity for all cases considered in this analysis.

The grid spacing Δx for all cases ensures 10 grid points within δ_{th}. As Karlovitz number can be scaled as $Ka \sim \delta_{th}^2/\eta^2$, the grid spacing Δx can be taken to be $\Delta x \le \delta_{th}/10 \sim \eta\sqrt{Ka}/10$. This indicates that $\eta/\Delta x \sim 10/\sqrt{Ka}$ assumes the smallest value in case P5 amongst the cases considered here as the value Ka is the highest in case P5. For case P5, Δx remained $\Delta x \sim \eta/2$ throughout the duration of the simulation. For other cases, the Kolmogorov scale is resolved by more than two grid points due to smaller value of Ka than in case P5. The above discussion suggests that the grid size chosen for the cases considered here is sufficient to resolve turbulence structures.

The thermophysical properties such as thermal conductivity (λ), dynamic viscosity (μ), and density-weighted mass diffusivity (ρD) are taken to be constant and independent of temperature in cases P1–P5, whereas these quantities in cases V1–V3 are taken to be temperature dependent and the temperature dependence approximated by 5th order polynomials following the CHEMKIN formats [40, 41]. It is worth noting that the cases P1–P5 and cases V1–V3 were originally developed independently (see [39] for cases P1–P5 and [40, 41] for cases V1–V3), but here these cases are considered together to assess if the SDR statistics obtained from DNS data with constant thermophysical properties in a canonical configuration remain qualitatively valid in a laboratory-scale configuration (e.g., V-flame configuration) with temperature-dependent thermophysical properties.

3. Results and Discussion

3.1. Flame-Turbulence Interaction. The contours of c in the central $x_1 - x_2$ plane for cases P1–P5 and V1–V3 are shown in Figures 1(a)–1(h), respectively. It is evident from Figures 1(a)–1(e) that the level of wrinkling increases with increasing $u'/S_L \sim Re_t^{1/4}Ka^{1/2} \sim Re_t^{1/2}/Da^{1/2}$. Turbulent eddies penetrate into the preheat zone in the thin reaction zones regime combustion ($Ka \sim \delta_{th}^2/\eta^2 \sim Re_t^{1/2}/Da > 1$), but the reaction zone remains unperturbed because the Kolmogorov length scale is larger than the reaction zone

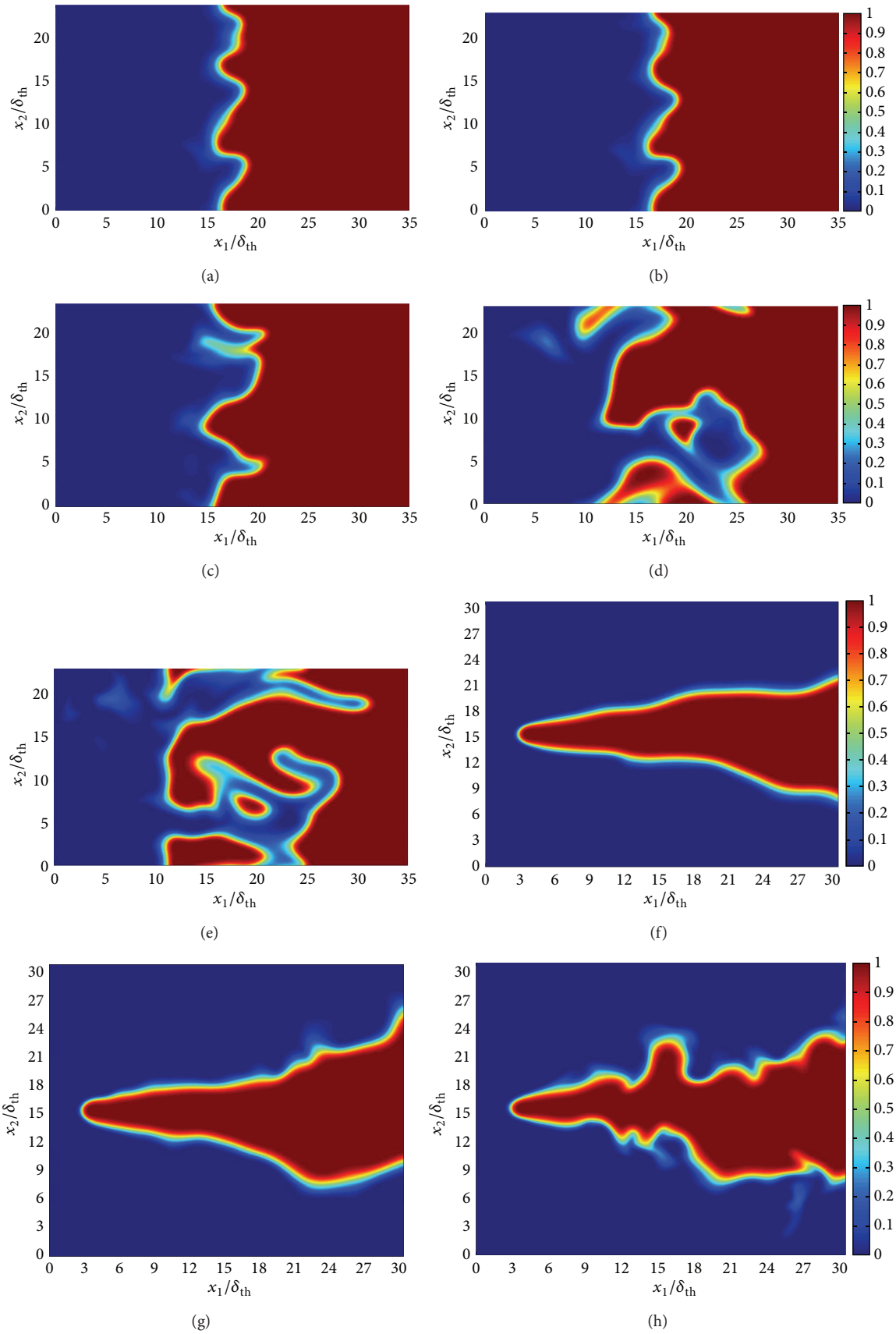

FIGURE 1: Distributions of c in the central $x_1 - x_2$ plane for cases P1–P5 (a–e) at $t_c = \delta_{th}/S_L$ and for cases V1–V3 (f–h).

thickness. The isosurfaces of c representing the preheat zone (i.e., $c \leq 0.5$) show more distortion than the isosurfaces representing the reaction zones (i.e., $0.7 \leq c \leq 0.9$) due to penetration of turbulent eddies within the preheat zone. However, this tendency is more prevalent for high values of u'/S_L and Ka (e.g., cases P3, P4, P5, and V3) but the isosurfaces of c remain mostly parallel to each other for small values of u'/S_L and Ka (e.g., cases P1, P2, V1, and V2) indicating that the internal flame structure is weakly affected by turbulence in these cases.

3.2. Statistical Behaviour of the Mean Values of N_c and the Unclosed Terms of Its Transport Equation. The variations of $\langle N_c \rangle \times \delta_{th}/S_L$ with c for statistically planar flames and V-flames are shown in Figures 2(a) and 2(b), where $\langle Q \rangle$ indicates the mean value of Q, which is obtained by ensemble averaging the quantity in question on a given c isosurface in the manner previously used by Boger et al. [42], Chakraborty and Cant [10, 11], and Chakraborty and Klein [15, 16]. It is worth noting that $\langle Q \rangle$ should not be confused with either Reynolds averaging or conventional conditional averaging operation in the context of RANS simulations because $\langle Q \rangle$ is evaluated using all the samples for a given c value over the whole domain. Figures 2(a) and 2(b) show that the variations of $\langle N_c \rangle \times \delta_{th}/S_L$ for statistically planar and V-flames are qualitatively similar to each other. For both statistically planar and V-flame configurations, the location of the maximum value of $\langle N_c \rangle \times \delta_{th}/S_L$ is skewed slightly towards the burned gas side of the flame (i.e., $c \approx 0.7$). The peak magnitude of $\langle N_c \rangle \times \delta_{th}/S_L$ does not change significantly in response to u'/S_L as the standard deviation for the case in the middle of the parameter range (i.e., cases P3 and V2) is found to exceed the difference in $\langle N_c \rangle \times \delta_{th}/S_L$ values for the cases considered here for both statistically planar and V-flame configurations. In order to understand the distribution of $\langle N_c \rangle \times \delta_{th}/S_L$ across the flame front, the variations of the mean values of the terms $\langle T_1 \rangle$, $\langle T_2 \rangle$, $\langle T_3 \rangle$, $\langle (-D_2) \rangle$, and $\langle f(D) \rangle$ conditional on c for planar and V-flames are shown in Figure 3. The variations of the mean values of the terms in cases P2, P3, and P4 (cases V2) are qualitatively similar to those in cases P1 and P5 (case V1) and thus are not explicitly shown here. It is evident from Figure 3 that the qualitative behaviour of these terms remains similar for all cases considered here. In all cases, $\langle T_1 \rangle$ remains positive throughout the flame. By contrast, $\langle (-D_2) \rangle$ assumes negative values throughout the flame in all cases as dictated by (1a). Expressing $\rho = \rho_0/(1 + \tau c)$ for low Mach number, unity Lewis number flames give rise to an alternative expression for T_1 [3, 17, 25, 28, 29]:

$$T_1 = 2\rho \frac{\partial u_j}{\partial x_j} N_c. \quad (4)$$

As dilatation rate $\partial u_j/\partial x_j$ is predominantly positive in premixed flames, $\langle T_1 \rangle$ for all values of c is positive across the flame and vanishes on both ends of the flame.

The quantity $\langle T_2 \rangle$ assumes negative values throughout the flame front for cases P1 and V1. Although $\langle T_2 \rangle$ remains negative for the major portion of the flame, small positive values can be discerned in cases P5 and V3. In order to understand this behaviour, the term T_2 can be expressed in the following manner [3, 22–24, 28, 30]:

$$T_2 = -2\rho N_c \left(e_\alpha \cos^2\alpha + e_\beta \cos^2\beta + e_\gamma \cos^2\gamma \right), \quad (5)$$

where e_α, e_β, and e_γ are the most extensive, intermediate, and most compressive principal strain rates and α, β, and γ are the angles of these principal strain rates with ∇c. Equation (5) demonstrates that the predominant alignment of e_α (e_γ) with ∇c leads to a negative (positive) contribution to T_2.

It has been discussed in the previous analyses [23, 24, 28, 30] that the alignment of ∇c with e_α and e_γ is determined by relative strengths of the strain rate induced by flame normal acceleration a_{chem} and turbulent straining a_{turb}. It has been demonstrated earlier that ∇c preferentially aligns with $e_\alpha(e_\gamma)$ when $a_{chem}(a_{turb})$ dominates over $a_{turb}(a_{chem})$. The strain rate induced by flame normal acceleration due to chemical heat release can be scaled as $a_{chem} \sim \tau f(\mathrm{Ka}) S_L/\delta_{th}$, where $f(\mathrm{Ka})$ is expected to decrease with increasing Ka [43]. Following Meneveau and Poinsot [44], a_{turb} can be scaled as $a_{turb} \sim u'/l$, which gives rise to $a_{chem}/a_{turb} \sim \tau f(\mathrm{Ka}) S_L l/u'\delta_{th} \sim \tau f(\mathrm{Ka})\mathrm{Da} \sim \tau f(\mathrm{Re}_t^{1/2}/\mathrm{Da})\mathrm{Da}$. Alternatively, turbulent straining can be scaled as [45] $a_{turb} \sim u'/\lambda$ (where λ is the Taylor microscale), which yields $a_{chem}/a_{turb} \sim \tau f(\mathrm{Ka}) S_L \lambda/u'\delta_{th} \sim \tau f(\mathrm{Ka})\mathrm{Da}/\mathrm{Re}_t^{1/2} \sim \tau f(\mathrm{Re}_t^{1/2}/\mathrm{Da})\mathrm{Da}/\mathrm{Re}_t^{1/2} \sim \tau f(\mathrm{Ka})/\mathrm{Ka}$. The above scaling relations suggest that a_{chem} strengthens with respect to a_{turb} with increasing Da for a given value of Re_t. Previous analyses [22–24, 28, 30] demonstrated that ∇c predominantly aligns with e_α for $\mathrm{Da} \gg 1$ flames, whereas ∇c aligns with e_γ in $\mathrm{Da} < 1$ flames for comparable values of Re_t. Both $a_{chem}/a_{turb} \sim \tau f(\mathrm{Ka})\mathrm{Da}$ and $a_{chem}/a_{turb} \sim \tau f(\mathrm{Re}_t^{1/2}/\mathrm{Da})\mathrm{Da}/\mathrm{Re}_t^{1/2} \sim \tau f(\mathrm{Ka})/\mathrm{Ka}$ indicate that an increase in $\mathrm{Ka} \sim \mathrm{Re}_t^{1/2}/\mathrm{Da}$ for a given value of Da (e.g., cases P1, P3, and P5) gives rise to weakening of a_{chem} in comparison to a_{turb}. This increases the extent of ∇c alignment with e_γ with increasing Ka when Da is held constant as in cases P1, P3, and P5. In cases P1 and P3, ∇c predominantly aligns with e_α; however the extent of this alignment decreases from P1 to P3. This predominant alignment of ∇c with e_α in cases P1 and P3 leads to a negative contribution of $\langle T_2 \rangle$ in these cases. In case P5, ∇c predominantly aligns with e_γ in the unburned and fully burned gases but a_{chem} overcomes a_{turb} in the regions of intense heat release close to the middle of the flame and as a result ∇c aligns with e_α in the reaction zone. Thus the mean value of $\langle T_2 \rangle$ in case P5 assumes positive values towards both the unburned and burned gas sides, whereas the mean contribution of $\langle T_2 \rangle$ remains negative close to the middle of the flame. The relation $a_{chem}/a_{turb} \sim \tau f(\mathrm{Ka})\mathrm{Da}/\mathrm{Re}_t^{1/2}$ indicates that a_{chem} weakens in comparison to a_{turb} with decreasing $\tau\mathrm{Da}/\mathrm{Re}_t^{1/2}$. The quantity $\tau\mathrm{Da}/\mathrm{Re}_t^{1/2}$ assumes values equal to 0.96, 0.55, and 0.49 for cases P2, P3, and P4, respectively, when the statistics were extracted. This leads to larger extent of ∇c aligning with e_γ in case P4 (case P3) than in case P3 (case P2). This leads to predominantly negative contribution of $\langle T_2 \rangle$ in cases P2 and P3, whereas $\langle T_2 \rangle$ assumes positive values towards the unburned and burned gas sides of the flame in case P4. However, a_{chem} overcomes a_{turb} in the regions of intense heat release at the middle of

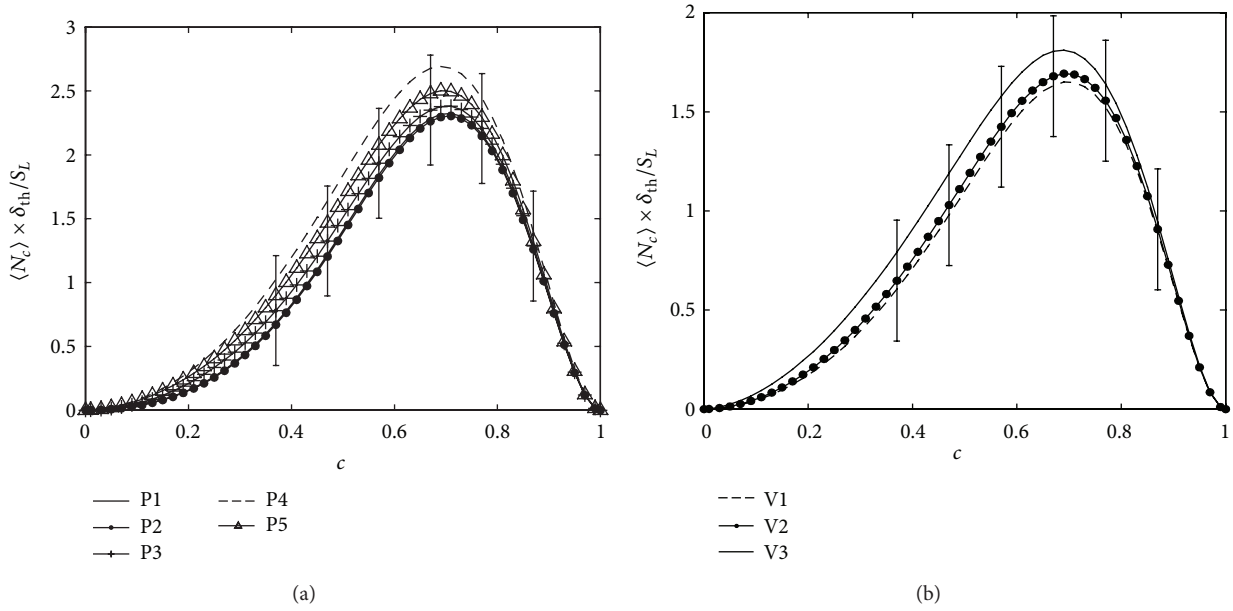

FIGURE 2: Variation of the mean value of $\langle N_c \rangle \times \delta_{th}/S_L$ conditional on c values across the flame front for (a) statistically planar cases with the bar indicating the standard deviation for case P3 and (b) V-flame cases with the bar indicating the standard deviation for case V2.

the flame and ∇c starts to align with e_α in the reaction zone giving rise to negative values of $\langle T_2 \rangle$ in case P4. In cases V1 and V2, the values of $a_{chem}/a_{turb} \sim \tau f(\text{Ka})\text{Da}/\text{Re}_t^{1/2}$ are larger than the corresponding value in case V3 (see the parameters in Table 1). Thus, the extent of ∇c alignment with $e_\alpha(e_\gamma)$ decreases (increases) from case V1 to case V3. This gives rise to positive values of $\langle T_2 \rangle$ towards both unburned and burned gas sides of the flame in case V3. This tendency is less prevalent in cases V1 and V2 due to smaller extent of ∇c alignment with e_γ than in case V3. However, the mean contribution of $\langle T_2 \rangle$ is negative in the middle of the flame for cases V1–V3 due to the alignment of ∇c with e_α in the heat releasing zone.

The contribution of $\langle T_3 \rangle$ remains positive (negative) towards the unburned (burned) gas side of the flame with the transition from positive to negative value taking place close to $c \approx 0.85$. In order to explain this behaviour, T_3 can be rewritten as

$$T_3 = -2Dn_i \frac{\partial \dot{w}}{\partial x_i} |\nabla c| = -2D \frac{\partial \dot{w}}{\partial n} |\nabla c|, \quad (6)$$

where n is the spatial coordinate in the local flame normal direction and the flame normal vector $\vec{n}$ points towards the unburned gas side of the flame. For single step chemistry considered here, the maximum $\dot{w}$ occurs close to $c \approx 0.85$ [10, 14]. This suggests that the probability of finding negative (positive) values of $\partial \dot{w}/\partial n$ is significant for $c < 0.85$ ($c > 0.85$), which gives rise to positive (negative) value of $\langle T_3 \rangle$ towards the unburned (burned) gas side of the flame.

Figure 3 shows that $\langle f(D) \rangle$ is weakly negative towards the unburned gas side before becoming positive towards the burned gas side in all the cases. The magnitude of the mean contribution of $\langle f(D) \rangle$ remains comparable to that of $\langle T_1 \rangle$ in all cases indicating that $\langle f(D) \rangle$ cannot be neglected even for cases P1–P5, where ρD is considered to be constant. In cases P1–P5, $\rho N_c[\partial D/\partial t + u_j \partial D/\partial x_j]$ can be expressed using $\rho = \rho_0/(1+\tau c)$ for globally adiabatic Le = 1.0 flames as $T_1/2 = \rho N_c \partial u_j/\partial x_j$ (i.e., $\rho N_c[\partial D/\partial t + u_j \partial D/\partial x_j] = \rho N_c(\partial u_j/\partial x_j)$ for constant ρD) and the first two terms on the right hand side of (1b) vanish for constant values of ρD. The contributions of $\langle (T_{D3} + T_{D4}) \rangle$ are responsible for the change in sign of $\langle f(D) \rangle$ in cases P1–P5. These terms are also principally responsible for sign change of $\langle f(D) \rangle$ in cases V1–V3.

3.3. Local Behaviour of N_c and Its Curvature and Strain Rate Dependences. The marginal probability density functions (pdfs) of normalised N_c^+ (i.e., $N_c \times \delta_{th}/S_L$) for different c iso-surfaces across the flame are shown in Figures 4(a) and 4(b) in log-log scale for cases P3 and V2, respectively. The pdfs of N_c in cases P1, P2, P4, and P5 (cases V1 and V3) are qualitatively similar to those in case P3 (case V2) and thus are not explicitly shown here. The pdfs for $c < 0.5$ are not shown in Figures 4(a) and 4(b), as N_c assumes small values in the preheat zone of the flame due to small magnitude of scalar gradient ∇c. It is evident from Figures 4(a) and 4(b) that the pdfs of N_c are qualitatively similar for statistically planar and V-flames and in both cases the probability of finding high values of N_c is most prevalent in the middle of the flame with slight skewness towards the burned gas side (i.e., $c \approx 0.7$) and the probability of finding high values of N_c decreases on both unburned and burned gas sides of the flame front. This is consistent with the observed behaviour of the mean values of N_c conditional on c shown in Figure 2. It can be seen in Figure 4 that a log-normal distribution captures the qualitative behaviour of the pdf of N_c although there are some disagreements in the pdf tails. This is consistent with several previous experimental [46–52] and numerical [53–55] studies

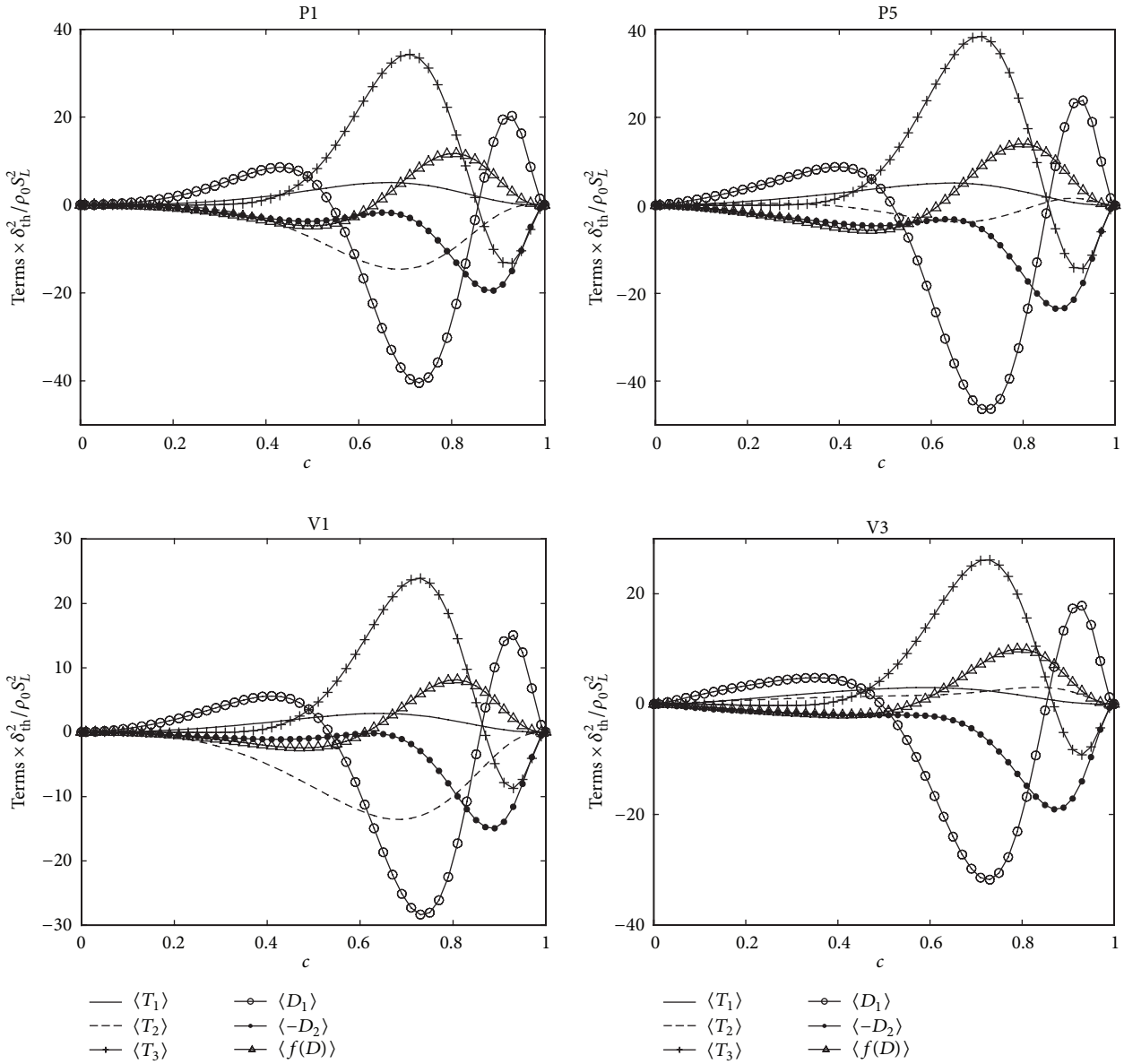

FIGURE 3: Variation of the mean values of $\langle T_1 \rangle$, $\langle T_2 \rangle$, $\langle T_3 \rangle$, $\langle -D_2 \rangle$, and $\langle f(D) \rangle$ conditional on c values across the flame for cases P1, P5, V1, and V3. All the terms of the transport equation of N_c are normalised with respect to the respective values of $\rho_0 S_L^2/\delta_{th}^2$.

investigating the scalar dissipation rate pdf of a passive scalar. An approximate log-normal distribution of SDR in turbulent premixed flames has also been reported in a previous analysis [56].

The joint pdfs of N_c and tangential strain rate a_T for cases P1, P5, V1, and V3 are shown in Figure 5(a) for $c = 0.8$ isosurface, which is close to the most reactive region for the present thermochemistry. It can be seen from Figure 5(a) that N_c and a_T are positively correlated on $c = 0.8$ isosurface for cases P1, P5, V1, and V3 and similar qualitative behaviour has been observed also for other c isosurfaces in all cases considered here. This positive correlation between N_c and a_T can be explained in the following manner.

(i) The dilatation rate $\nabla \cdot \vec{u}$ can be expressed as $\nabla \cdot \vec{u} = a_T + a_n$, where $a_n = n_i n_j \partial u_i / \partial x_j$ is the normal strain rate. For unity Lewis number flames, $\nabla \cdot \vec{u}$ can be scaled as $\nabla \cdot \vec{u} \sim a_{chem} \sim \tau f(\mathrm{Ka}) S_L/\delta_{th}$, whereas a_T can be taken to scale with turbulent strain rate a_{turb} (i.e., $a_T \sim a_{turb} \sim u'/l$ according to Meneveau and Poinsot [44] and $a_T \sim a_{turb} \sim u'/\lambda$ according to Tennekes and Lumley [45]).

(ii) Above scalings indicate that $\nabla \cdot \vec{u}/a_T$ scales as $\nabla \cdot \vec{u}/a_T \sim \tau f(\mathrm{Re}_t^{1/2}/\mathrm{Da})\mathrm{Da}$ and $\nabla \cdot \vec{u}/a_T \sim \tau f (\mathrm{Re}_t^{1/2}/\mathrm{Da})\ \mathrm{Da}/\mathrm{Re}_t^{1/2} \sim \tau f(\mathrm{Ka})/\mathrm{Ka}$ according to the scaling arguments by Meneveau and Poinsot [44] and Tennekes and Lumley [45], respectively. Both

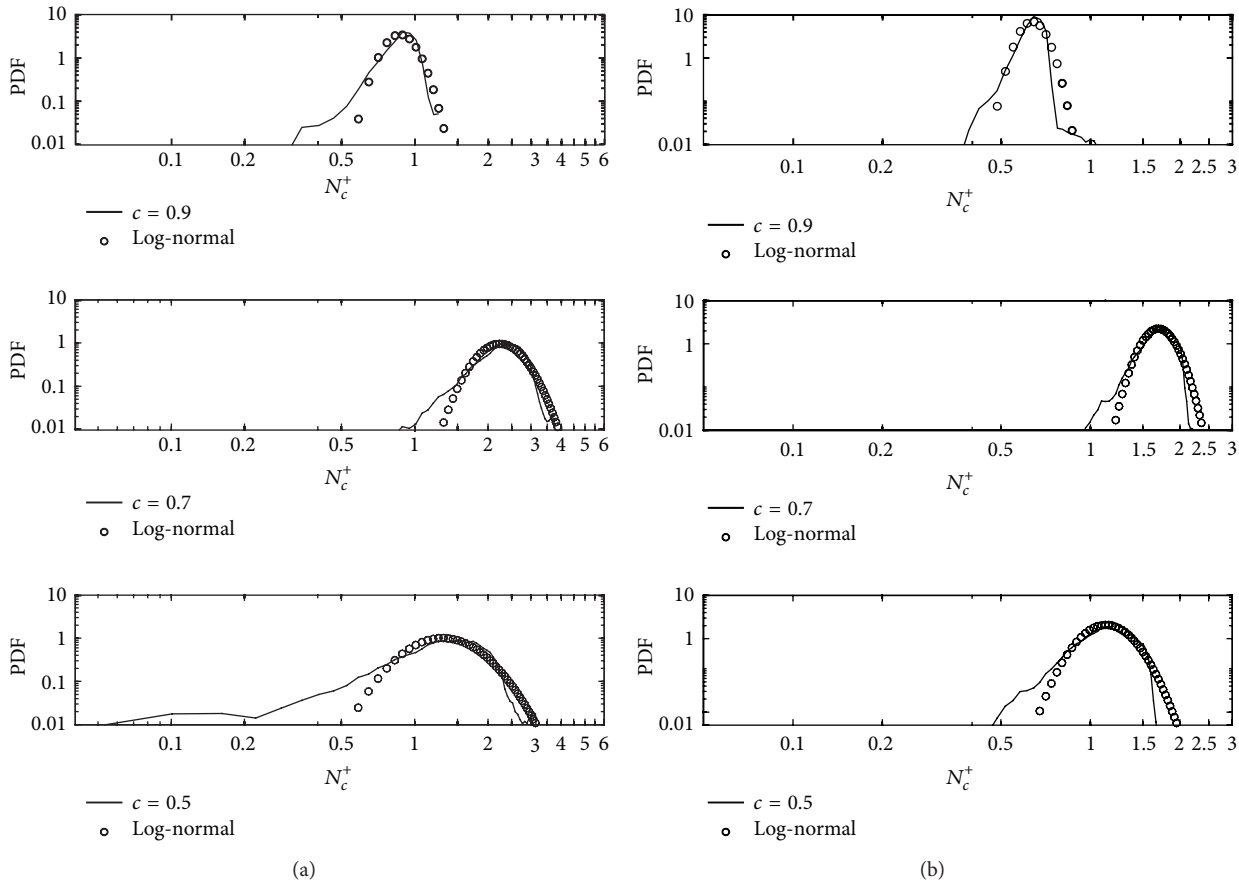

FIGURE 4: The marginal pdf of normalised N_c^+ (i.e., $N_c \times \delta_{th}/S_L$) and the log-normal distribution in log-log scale for $c = 0.5$, 0.7, and 0.9 across the flame for cases (a) P3 and (b) V2.

$\nabla \cdot \vec{u}/a_T \sim \tau f(\mathrm{Re}_t^{1/2}/\mathrm{Da})\mathrm{Da}$ and $\nabla \cdot \vec{u}/a_T \sim \tau f(\mathrm{Re}_t^{1/2}/\mathrm{Da})\ \mathrm{Da}/\mathrm{Re}_t^{1/2} \sim \tau f(\mathrm{Ka})/\mathrm{Ka}$ suggest that the magnitude of a_T is likely to supersede the magnitude of $\nabla \cdot \vec{u}$ in most locations within the flame for small values of Da and high values of Ka.

(iii) It has been shown in several previous analyses [10, 30] that both $\nabla \cdot \vec{u}$ and a_T assume predominantly positive values and thus a higher magnitude of a_T than $\nabla \cdot \vec{u}$ induces a negative (i.e., compressive) normal strain rate a_n. Thus, an increase in a_T often leads to a decrease in $a_n = \nabla \cdot \vec{u} - a_T$ for small (high) values of Da (Ka). Thus, the isoscalar lines come close to each other under the action of decreasing a_n, which leads to increase in the magnitude of scalar gradient ∇c. This is reflected in the positive correlation between N_c and a_T.

The joint pdfs between N_c and curvature κ_m for cases P1, P5, V1, and V3 are shown in Figure 5(b) for $c = 0.8$ isosurface. Cases P2 and P3 (case V2) are not explicitly shown here due to their similarities to cases P1 and P5 (case V1), respectively. It can be seen from Figure 5(b) that the joint pdf between N_c and κ_m exhibits both positive and negative correlating branches on $c = 0.8$ isosurface for cases P5 and V3, and as a result of this, the net correlation between N_c and κ_m remains weak. The positive correlation branch between N_c and κ_m remains weak for small values of u'/S_L in statistically planar flames (see Figure 5(b) for case P1) and this branch disappears completely in the V-flames with small values of u'/S_L (see Figure 5(b) for case V1). Similar behaviour is observed for other c isosurfaces in all cases considered here and the correlation between N_c and κ_m is weak throughout the flame for high values of u'/S_L (e.g., cases P3–P5 and V3). However, the disappearance of the positive correlating branch in the joint pdf of N_c and κ_m in Figure 5(b) indicates that N_c and κ_m are negatively correlated with each other throughout the flame for small values of u'/S_L (e.g., cases P1, P2, V1, and V2). The observed behaviour can be explained based on the following physical mechanisms.

(i) Previous analyses (e.g., [57]) demonstrated that both a_T and $\nabla \cdot \vec{u}$ remain negatively correlated with κ_m in turbulent premixed flames, and thus the behaviour of a_n at locations with large positive curvature is principally determined by a_T since $\nabla \cdot \vec{u}$ is small in these zones due to defocusing of heat. Small values of a_T are associated with high values of κ_m at these locations, which lead to small values of N_c at high values of positive κ_m due to positive correlation between N_c

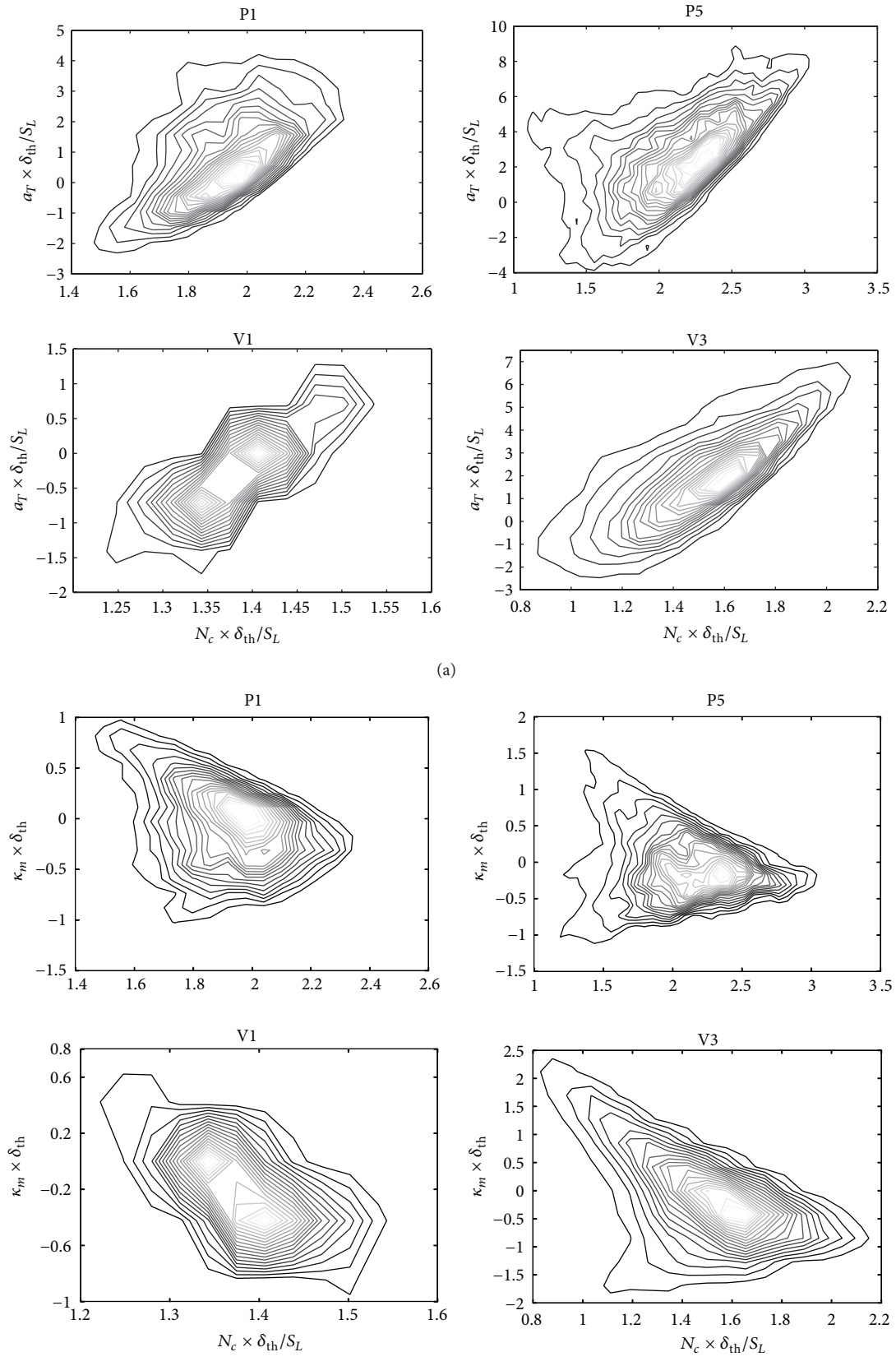

FIGURE 5: (a) Joint pdfs between $N_c \times \delta_{th}/S_L$ and normalised tangential strain rate $a_T \times \delta_{th}/S_L$ on $c = 0.8$ isosurface for cases P1, P5, V1, and V3. (b) Joint pdf between $N_c \times \delta_{th}/S_L$ and normalised curvature $\kappa_m \times \delta_{th}$ on $c = 0.8$ isosurface for cases P1, P5, V1, and V3.

and a_T. This leads to a negative correlating branch between N_c and κ_m at the positively curved zones.

(ii) The dilatation rate $\nabla \cdot \vec{u}$ is large in the negatively curved locations due to strong focussing of heat and the magnitude of $\nabla \cdot \vec{u}$ can locally be high enough to supersede the magnitude of a_T, which leads to a positive value of a_n. This tendency strengthens with decreasing κ_m, especially in the zones with large negative curvature, which gives rise to an increase in a_n with decreasing curvature. As the distance between the isoscalar lines increases with increasing a_n, the magnitude of scalar gradient ∇c decreases with decreasing κ_m in the negatively curved zones. This leads to the positive correlating branch in the joint pdf of N_c and κ_m (see Figure 5(b) for cases P5 and V3).

(iii) The relative strengths of the positive and negative correlating branches ultimately determine the net correlation between N_c and κ_m in the high u'/S_L cases. The probability of finding high negative curvature remains small for small values of u'/S_L and as a result the probability of finding high values of $\nabla \cdot \vec{u}$, which locally overcomes a_T, to induce a positive value of a_n, becomes rare (e.g., cases P1 and V1). Thus the combination of positive correlations between N_c and a_T and negative correlations between a_T and κ_m leads to a predominantly negative correlating branch between N_c and κ_m in the low u'/S_L cases (e.g., cases P1 and V1; see Figure 5(b)).

The strain rate and curvature dependences of N_c discussed above, in turn, affect the local statistical behaviours of T_1, T_2, T_3, $(-D_2)$, and $f(D)$ in response to a_T and κ_m. The curvature and strain rate dependences of T_1, T_2, T_3, $(-D_2)$, and $f(D)$ are discussed next.

3.4. Local Behaviour of T_1 and Its Curvature and Strain Rate Dependences. The marginal pdfs of T_1 for different c isosurfaces across the flame are shown in Figures 6(a) and 6(b) for cases P3 and V2, respectively. The pdfs of T_1 in cases P1, P2, P4, and P5 (cases V1 and V3) are qualitatively similar to those in case P3 (case V2) and thus are not explicitly shown here. It is evident from Figures 6(a) and 6(b) that the pdfs of T_1 are qualitatively similar for statistically planar and V-flames and in both cases $T_1 = 2\rho(\nabla \cdot \vec{u})N_c$ assumes predominantly positive values throughout the flame. As dilatation rate $\nabla \cdot \vec{u}$ is principally positive due to thermal expansion in premixed flames [10, 30], the contribution of $T_1 = 2\rho(\nabla \cdot \vec{u})N_c$ is predominantly positive throughout the flame. Moreover, Figures 6(a) and 6(b) demonstrate that the probability of finding high values of T_1 is most prevalent in the middle of the flame with slight skewness towards the burned gas side (i.e., $c \approx 0.7$) and the probability of finding high values of T_1 decreases on both unburned and burned gas sides of the flame. This is consistent with the observed behaviour of the mean values of T_1 conditional on c shown in Figure 3. The probability of finding large magnitudes of $\nabla \cdot \vec{u}$ is the highest at a location which is slightly skewed towards the burned gas side of the flame [30]. As the distributions of N_c and $\nabla \cdot \vec{u}$ are slightly skewed towards the burned gas side of the flame, the probability of finding large values of $T_1 = 2\rho(\nabla \cdot \vec{u})N_c$ becomes high around $c \approx 0.7$.

The joint pdfs between T_1 and a_T for cases P3 and V2 are shown in Figures 6(c) and 6(d), respectively, for $c = 0.8$ isosurface. It can be seen from Figures 6(c) and 6(d) that T_1 and a_T are positively correlated on $c = 0.8$ isosurface for cases P3 and V2 and similar qualitative behaviours have been observed for other c isosurfaces in all cases considered here. Both $\nabla \cdot \vec{u}$ and a_T are positively correlated for all flames considered here, which along with positive correlation between N_c and a_T (see Figure 5) gives rise to a positive correlation between $T_1 = 2\rho(\nabla \cdot \vec{u})N_c$ and a_T.

The joint pdfs between T_1 and κ_m for cases P3 and V2 are shown in Figures 6(e) and 6(f), respectively, for $c = 0.8$ isosurface. It can be seen from Figures 6(e) and 6(f) that the joint pdf between T_1 and κ_m exhibits a negative correlation on $c = 0.8$ isosurface for cases P3 and V2, and similar qualitative behaviour has been observed for other c isosurfaces in all cases considered here. In all cases, the net correlation between N_c and κ_m is weak (see Figure 5(b)), but $\nabla \cdot \vec{u}$ assumes high (small) values at negatively (positively) curved locations because of focussing (defocusing) of heat. This leads to a predominantly negative correlation between $\nabla \cdot \vec{u}$ and κ_m [57]. The negative correlation between $\nabla \cdot \vec{u}$ and κ_m is principally responsible for the negative correlation between $T_1 = 2\rho(\nabla \cdot \vec{u})N_c$ and κ_m.

3.5. Local Behaviour of T_2 and Its Curvature and Strain Rate Dependences. The marginal pdfs of T_2 for different c isosurfaces across the flame are shown in Figures 7(a) and 7(b) for cases P3 and V2, respectively. The pdfs of T_2 in cases P1, P2, P4, and P5 (cases V1 and V3) are qualitatively similar to those in case P3 (case V2) and thus are not explicitly shown here. Figures 7(a) and 7(b) show that the probability of finding negative values of T_2 supersedes the probability of finding positive values. The probability of finding negative values of T_2 increases as the heat releasing zone (see the pdfs for $c = 0.7$ isosurface) is approached. It has been discussed earlier that the effects of a_{chem} overcome the effects of a_{turb} in the heat releasing zone to give rise to a preferential alignment of ∇c with e_α even for small values of Da. This preferential alignment of ∇c with e_α in these zones gives rise to negative values of T_2 according to (5). The extent of ∇c alignment with $e_\alpha(e_\gamma)$ decreases (increases) towards both unburned and burned gas sides of the flame due to diminishing effects of a_{chem}.

The contours of joint pdfs between T_2 and a_T for $c = 0.8$ are shown in Figures 7(c) and 7(d) for cases P3 and V2 and the correlation coefficients between T_2 and a_T for different c isosurfaces across the flame for all cases are shown in Table 2. It is evident from Figures 7(c) and 7(d) and Table 2 that T_2 and a_T are positively correlated for high u'/S_L cases (e.g., cases P5 and V3) although the strength of the correlation changes through the flame. However, T_2 and a_T are weakly correlated with each other within the flame, where the effects of heat release are significant for cases with small and moderate values of u'/S_L (see Table 2). In order to explain

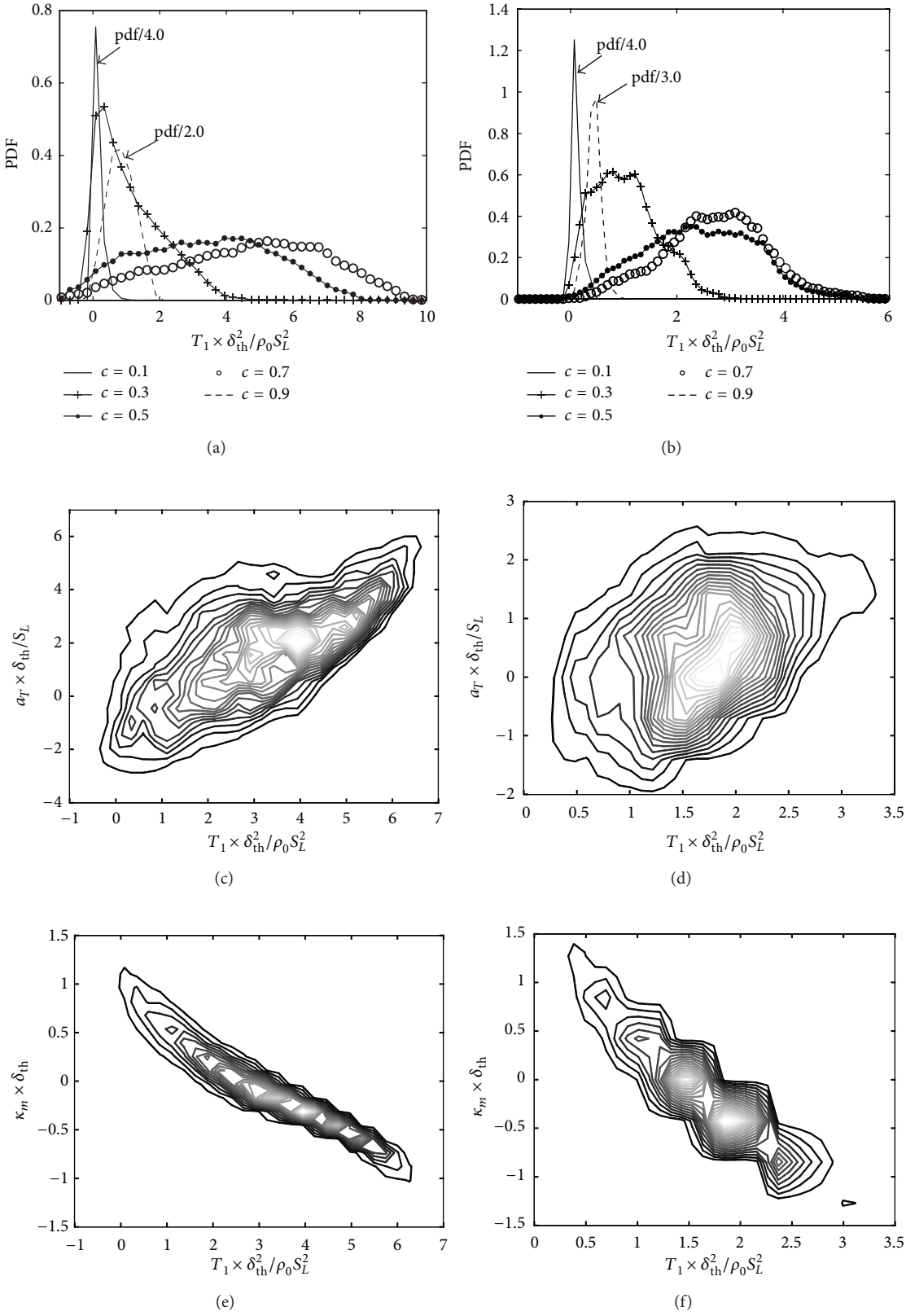

FIGURE 6: The marginal pdfs of $T_1 \times \delta_{th}^2/\rho_0 S_L^2$ for $c = 0.1$, 0.3, 0.5, 0.7, and 0.9 for cases (a) P3 and (b) V2. Joint pdf between $T_1 \times \delta_{th}^2/\rho_0 S_L^2$ and normalised tangential strain rate $a_T \times \delta_{th}/S_L$ on $c = 0.8$ isosurface for cases (c) P3 and (d) V2. Joint pdf between $T_1 \times \delta_{th}^2/\rho_0 S_L^2$ and normalised curvature $\kappa_m \times \delta_{th}$ on $c = 0.8$ isosurface for cases (e) P3 and (f) V2.

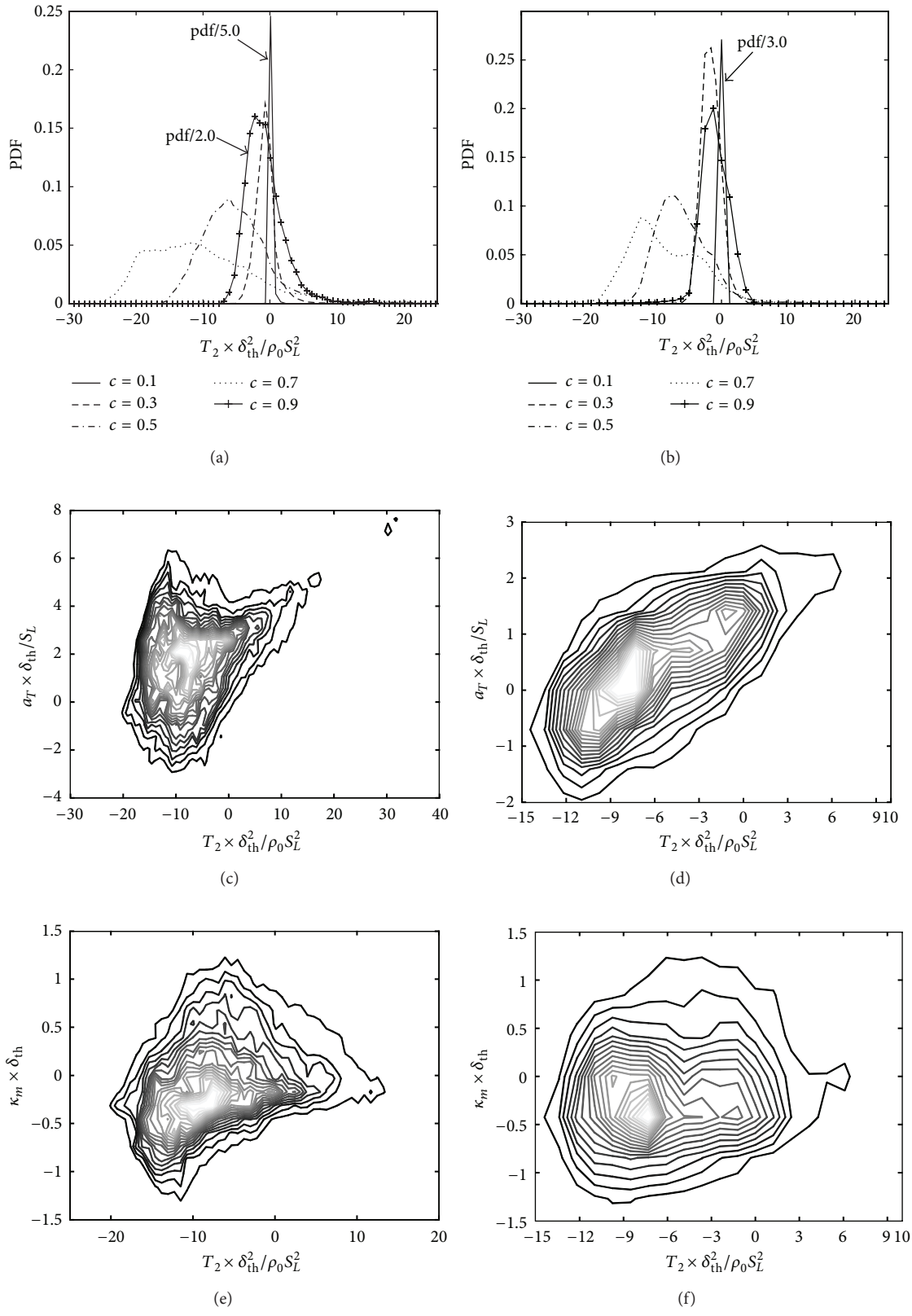

FIGURE 7: The marginal pdfs of $T_2 \times \delta_{th}^2/\rho_0 S_L^2$ for $c = 0.1$, 0.3, 0.5, 0.7, and 0.9 for cases (a) P3 and (b) V2. Joint pdf between $T_2 \times \delta_{th}^2/\rho_0 S_L^2$ and normalised tangential strain rate $a_T \times \delta_{th}/S_L$ on $c = 0.8$ isosurface for cases (c) P3 and (d) V2. Joint pdf between $T_2 \times \delta_{th}^2/\rho_0 S_L^2$ and normalised curvature $\kappa_m \times \delta_{th}$ on $c = 0.8$ isosurface for cases (e) P3 and (f) V2.

Table 2: Correlation coefficients between T_2 and a_T and between T_2 and κ_m on $c = 0.1$, 0.3, 0.5, 0.7, and 0.9 isosurfaces.

Case	$T_2 - a_T$					$T_2 - \kappa_m$				
	$c = 0.1$	$c = 0.3$	$c = 0.5$	$c = 0.7$	$c = 0.9$	$c = 0.1$	$c = 0.3$	$c = 0.5$	$c = 0.7$	$c = 0.9$
P1	0.642	−0.098	−0.217	−0.092	0.685	0.141	0.509	0.720	0.614	−0.250
P2	0.673	−0.090	−0.208	−0.084	0.676	0.116	0.506	0.719	0.616	−0.227
P3	0.751	0.376	0.263	0.263	0.648	0.544	0.252	0.412	0.423	−0.065
P4	0.802	0.593	0.616	0.689	0.827	0.052	0.196	0.235	0.198	−0.027
P5	0.783	0.662	0.614	0.616	0.787	0.028	0.137	0.223	0.242	−0.014
V1	0.245	0.367	0.749	0.816	0.971	0.612	0.623	0.354	0.135	−0.043
V2	0.591	0.335	0.495	0.699	0.920	0.345	0.565	0.497	0.328	−0.067
V3	0.767	0.721	0.738	0.768	0.888	−0.009	0.057	0.077	0.028	−0.155

this behaviour, it is useful to rewrite T_2 in the following manner:

$$T_2 = -2\rho a_n N_c. \tag{7}$$

Based on (7) the strain rate dependences of T_2 can be explained in the following manner.

(i) It has already been demonstrated that N_c and a_T are positively correlated with each other (see Figure 5(a)). The quantity $(-a_n) = a_T - \nabla \cdot \vec{u}$ tends to increase with increasing a_T in the regions where the effects of $\nabla \cdot \vec{u}$ are weak. This along with positive correlation between N_c and a_T leads to a positive correlation between T_2 and a_T for both unburned and burned gas sides of the flame for all cases.

(ii) The magnitudes of $\nabla \cdot \vec{u}$ and a_T increase with decreasing κ_m, and thus $(-a_n) = a_T - \nabla \cdot \vec{u}$ might not increase (even decrease) with increasing a_T in the heat releasing zone of the flame where the effects of $\nabla \cdot \vec{u}$ are strong. The a_T dependences of $(-a_n)$ and N_c ultimately determine the nature of the correlation between T_2 and a_T. The strain rate and curvature dependences of $\nabla \cdot \vec{u}$ weaken with increasing u'/S_L [58], so $(-a_n) = a_T - \nabla \cdot \vec{u}$ increases with increasing a_T, which leads to a positive correlation between T_2 and a_T for the major portion of the flame for cases with high values of u'/S_L (see Table 2).

The joint pdfs between T_2 and κ_m for cases P3 and V2 are shown in Figures 7(e) and 7(f), respectively, for $c = 0.8$ isosurface and the correlation coefficients between T_2 and κ_m for different c isosurfaces across the flame are shown in Table 2 for all cases considered here. It is evident from Figures 7(e) and 7(f) and Table 2 that T_2 and κ_m remain weakly positively correlated except the burned gas side of the flame. The observed curvature dependence of T_2 could be explained based on the following physical mechanisms.

(i) The effects of dilatation rate $\nabla \cdot \vec{u}$ and thermal expansion are particularly strong in the negatively curved regions due to focussing of heat. By the same token, the effects of heat release are weak in the positively curved zones due to defocusing of heat. Thus, the effects of a_{chem} are more likely to dominate over the effects of a_{turb} in the negatively curved zones, which increase the extent of ∇c alignment with e_α as demonstrated earlier by Hartung et al. [58]. Weakening of the heat release effects at positively curved zones due to defocusing of heat leads to a greater (lesser) extent of ∇c alignment with $e_\gamma (e_\alpha)$ in the positively curved zones. The extent of ∇c alignment with e_α increases in the negatively curved zones, which in turn makes T_2 increasingly negative (see (5)) and the magnitude of the negative contribution of T_2 decreases for positive curvature locations. This gives rise to a positive correlation between T_2 and κ_m, as observed from Figures 7(e) and 7(f) and Table 2.

(ii) However, the effects of a_{turb} are more likely to dominate over the effects of a_{chem} towards the burned gas side and thus the extent of ∇c alignment with e_γ is determined by local turbulent flow conditions. The effects of flame-generated turbulence become stronger at the negatively curved zones due to stronger thermal expansion effects resulting from focussing of heat especially in the heat releasing zone. The straining induced by flame-generated turbulence may overcome relatively weak effects of $\nabla \cdot \vec{u}$ towards the burned gas side, which can give rise to an increasing extent of ∇c alignment with e_γ increases in the negative curved zones. This in turn gives rise to an increase in T_2 (see (5)) with decreasing κ_m towards the burned gas side and leads to a negative correlation between T_2 and κ_m (see Table 2).

3.6. Local Behaviour of T_3 and Its Curvature and Strain Rate Dependences. The marginal pdfs of normalised T_3 for different c isosurfaces across the flame are shown in Figure 8 for cases P3 and V2, respectively. The pdfs of T_3 in cases P1, P2, P4, and P5 (cases V1 and V3) are qualitatively similar to those in case P3 (case V2) and thus are not explicitly shown here. The pdfs for $c < 0.5$ are not shown in Figure 8 because T_3 assumes negligible value in the preheat zone of the flame due to negligible magnitude of $\dot{w}$. It is evident that T_3 assumes positive values for the major portion of the flame for both statistically planar and V-flames and the probability of finding high positive values increases towards the most reactive zone (e.g., $c = 0.7$ in Figure 8) of the flame front. However, T_3 assumes negative values only towards the burned gas side

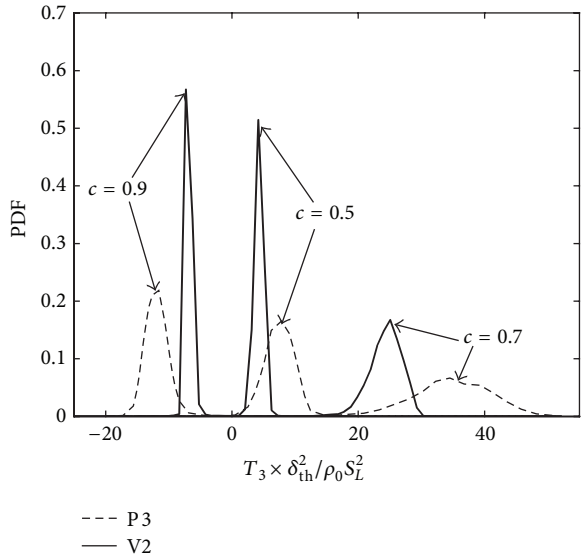

FIGURE 8: The marginal pdfs of $T_3 \times \delta_{th}^2/\rho_0 S_L^2$ for $c = 0.5$, 0.7, and 0.9 for cases P3 and V2.

(e.g., $c = 0.9$) of the flame front for both planar and V-flames. This is consistent with the behaviour of $\langle T_3 \rangle$ shown in Figure 3. The physical mechanism behind the transition from positive to negative values of the mean contribution of T_3 (see (6)) is also responsible for obtaining negative (positive) values of T_3 towards the burned (unburned) gas side of the flame.

The contours of joint pdfs between T_3 and a_T for $c = 0.5$, 0.7, and 0.9 isosurfaces are shown in Figures 9(a)–9(f) for cases P3 and V2 and similar qualitative behaviour has been observed for other cases considered here. It is evident from Figures 9(a)–9(f) that T_3 and a_T remain positively correlated for the part of the flame where finding positive values of T_3 is prevalent. On the other hand, T_3 and a_T are negatively correlated with each other towards the burned gas side of the flame where T_3 is predominantly negative. The observed a_T dependence of T_3 can be explained in the following manner.

(i) It has been demonstrated earlier that N_c and a_T are positively correlated with each other which suggests that $|\nabla c| = |\partial c/\partial n|$ increases with increasing a_T. For low Mach number, unity Lewis number flames $\dot{w}$ depend only on c and thus high values of $|\partial \dot{w}/\partial n|$ are associated with high values of $|\nabla c| = |\partial c/\partial n|$ and N_c.

(ii) As N_c and a_T are positively correlated with each other, the magnitude of reaction rate contribution $|T_3| = |2D(\partial \dot{w}/\partial n)|\nabla c||$ is positively correlated with tangential strain rate a_T. Thus, T_3 is positively (negative) correlated with a_T, where T_3 assumes positive (negative) values.

The joint pdfs between T_3 and κ_m for cases P3 and V2 are shown in Figure 10 for $c = 0.5$, 0.7, and 0.9 isosurfaces and similar qualitative behaviour has been observed for other cases considered here. It is evident from Figure 10 that the joint pdf of T_3 and κ_m exhibits both positive and negative correlating branches and the net correlation is weak throughout the flame. The physical explanations for the observed κ_m dependence of T_3 can be summarised in the following manner.

(i) The term $|T_3| = |2D(\partial \dot{w}/\partial n)|\nabla c||$ is expected to be positively (negatively) correlated with curvature κ_m at negatively (positively) curved locations for high values of u'/S_L, as in the case of N_c (see cases P5 and V3 in Figure 5(b)), because high values of $|\partial \dot{w}/\partial n|$ are associated with high values of N_c and $|\nabla c| = |\partial c/\partial n|$.

(ii) As a result of the aforementioned physical mechanisms, the term T_3 and κ_m remain positively (negatively) correlated with curvature κ_m at negatively (positively) curved locations in the planar flames where T_3 assumes positive values. By contrast, the joint pdfs of T_3 and κ_m exhibit negative (positive) correlation with curvature κ_m at negatively (positively) curved locations within the flame where T_3 assumes negative values for the planar flames considered here (see Figure 10(c)). However, N_c remains predominantly negatively correlated with κ_m for V-flame cases (see Figure 5(b)) and thus T_3 shows positive (negative) correlation with curvature where T_3 assumes negative (positive) values (see Figures 10(d)–10(f)).

3.7. Local Behaviour of $(-D_2)$ and Its Curvature and Strain Rate Dependences. The marginal pdfs of $(-D_2)$ for c isosurfaces representative of leading edge, reaction zone, and trailing edge of the flame (e.g., $c = 0.3$, 0.7 and 0.9 isosurfaces) are shown in Figure 11(a) for cases P3 and V2. The pdfs of $(-D_2)$ in cases P1, P2, P4, and P5 (cases V1 and V3) are qualitatively similar to that in case P3 (case V2) and thus are not explicitly shown here. Figure 11(a) shows that $(-D_2)$ assumes negative values throughout the flame and the probability of finding high magnitude of $(-D_2)$ increases from unburned gas side towards a region of the flame which is severely skewed towards the burned gas side (e.g., $c = 0.9$ isosurface). This behaviour is found to be consistent with the mean behaviour of $(-D_2)$ shown in Figure 3. It can further be seen from Figure 11(a) that the pdfs of $(-D_2)$ for statistically planar and V-flames are qualitatively similar to each other.

The contours of joint pdfs between $(-D_2)$ and a_T for $c = 0.8$ isosurface are shown in Figures 11(b) and 11(c) for cases P3 and V2 and the correlation coefficients between $(-D_2)$ and a_T for different c isosurfaces across the flame for all cases considered here are shown in Table 3. Figures 11(b) and 11(c) and Table 3 show that $(-D_2)$ and a_T are predominantly negatively correlated throughout the flame but the strength of this negative correlation weakens with increasing u'/S_L and the correlation becomes weakly positive at the middle of the flame for high values of u'/S_L (e.g., cases P4 and P5). This behaviour can be explained in the following manner.

(i) The instantaneous SDR N_c and the molecular dissipation term $(-D_2)$ can be taken to scale as $N_c \sim D/\delta^2$ and $(-D_2) \sim (-\rho D^2/\delta^4) \sim (-\rho N_c^2)$ (where δ is the typical local flame thickness) because in premixed flames. the gradient of progress variable is

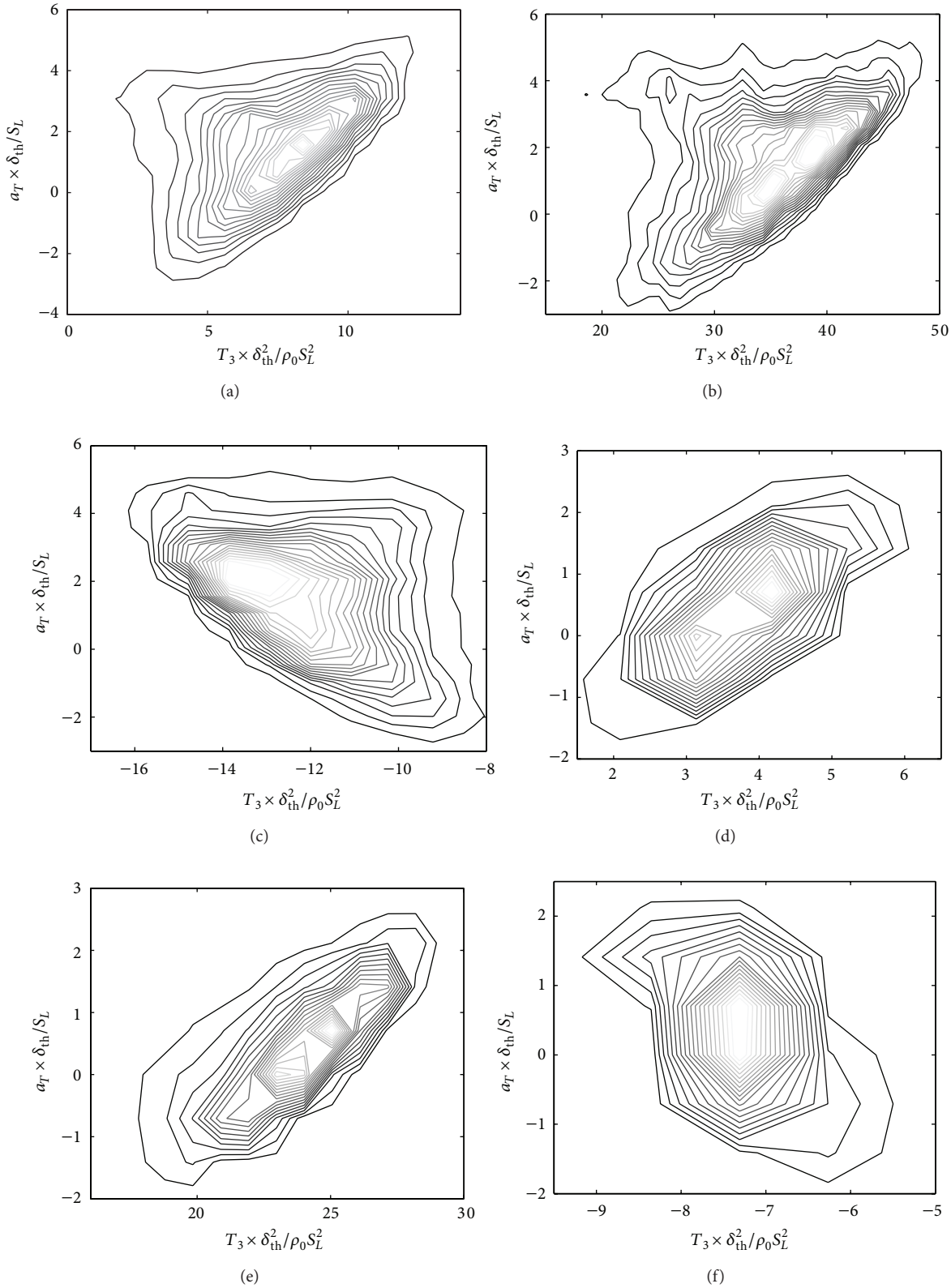

FIGURE 9: Joint pdfs between $T_3 \times \delta_{th}^2/\rho_0 S_L^2$ and normalised tangential strain rate $a_T \times \delta_{th}/S_L$ on (a) $c = 0.5$, (b) 0.7, and (c) 0.9 isosurfaces for case P3. Joint pdfs between $T_3 \times \delta_{th}^2/\rho_0 S_L^2$ and normalised tangential strain rate $a_T \times \delta_{th}/S_L$ on (d) $c = 0.5$, (e) 0.7, and (f) 0.9 isosurfaces for case V2.

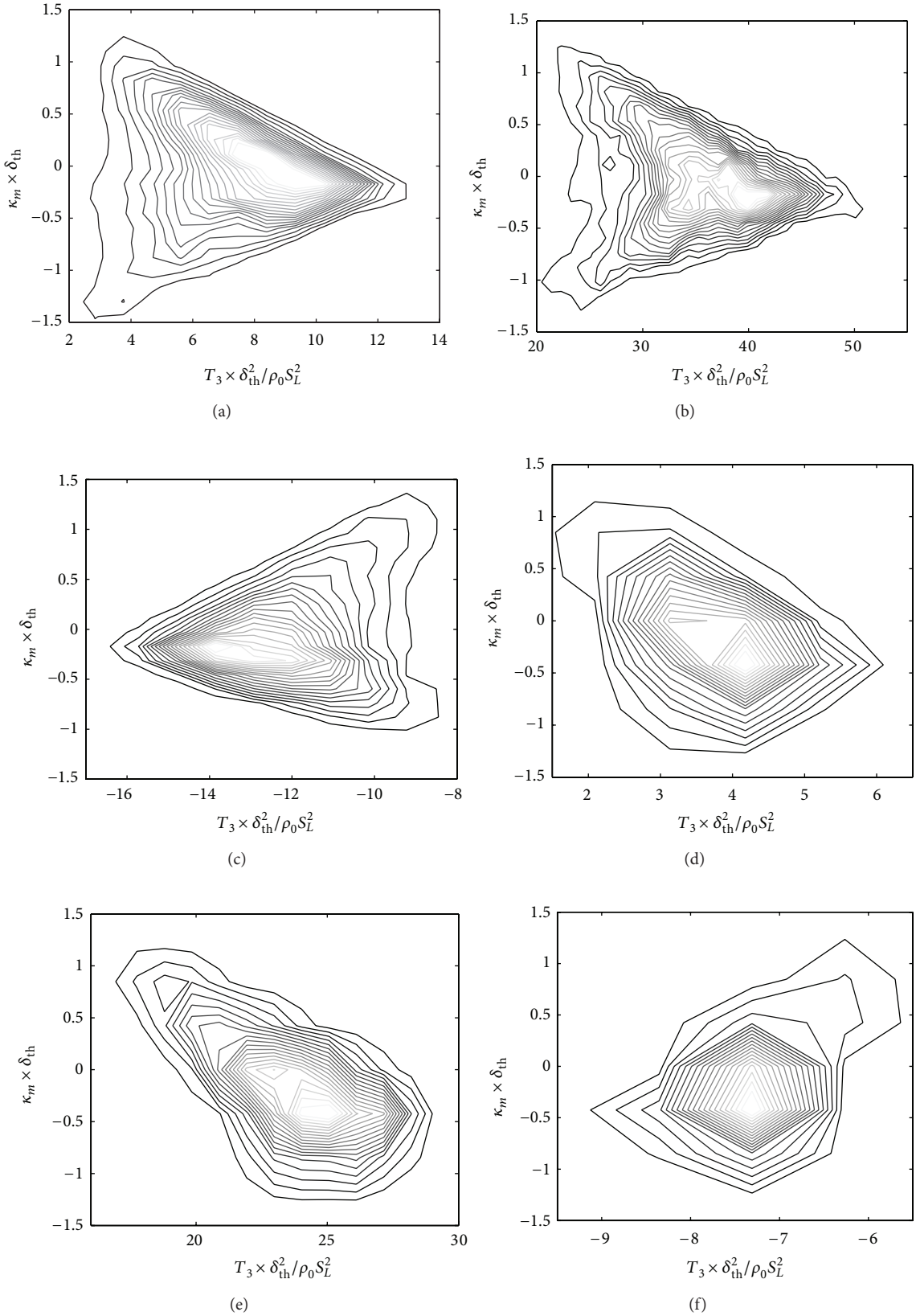

FIGURE 10: Joint pdfs between $T_3 \times \delta_{\text{th}}^2/\rho_0 S_L^2$ and normalised curvature $\kappa_m \times \delta_{\text{th}}$ on (a) $c = 0.5$, (b) 0.7, and (c) 0.9 isosurfaces for case P3. Joint pdfs between $T_3 \times \delta_{\text{th}}^2/\rho_0 S_L^2$ and normalised curvature $\kappa_m \times \delta_{\text{th}}$ on (d) $c = 0.5$, (e) 0.7, and (f) 0.9 isosurfaces for case V2.

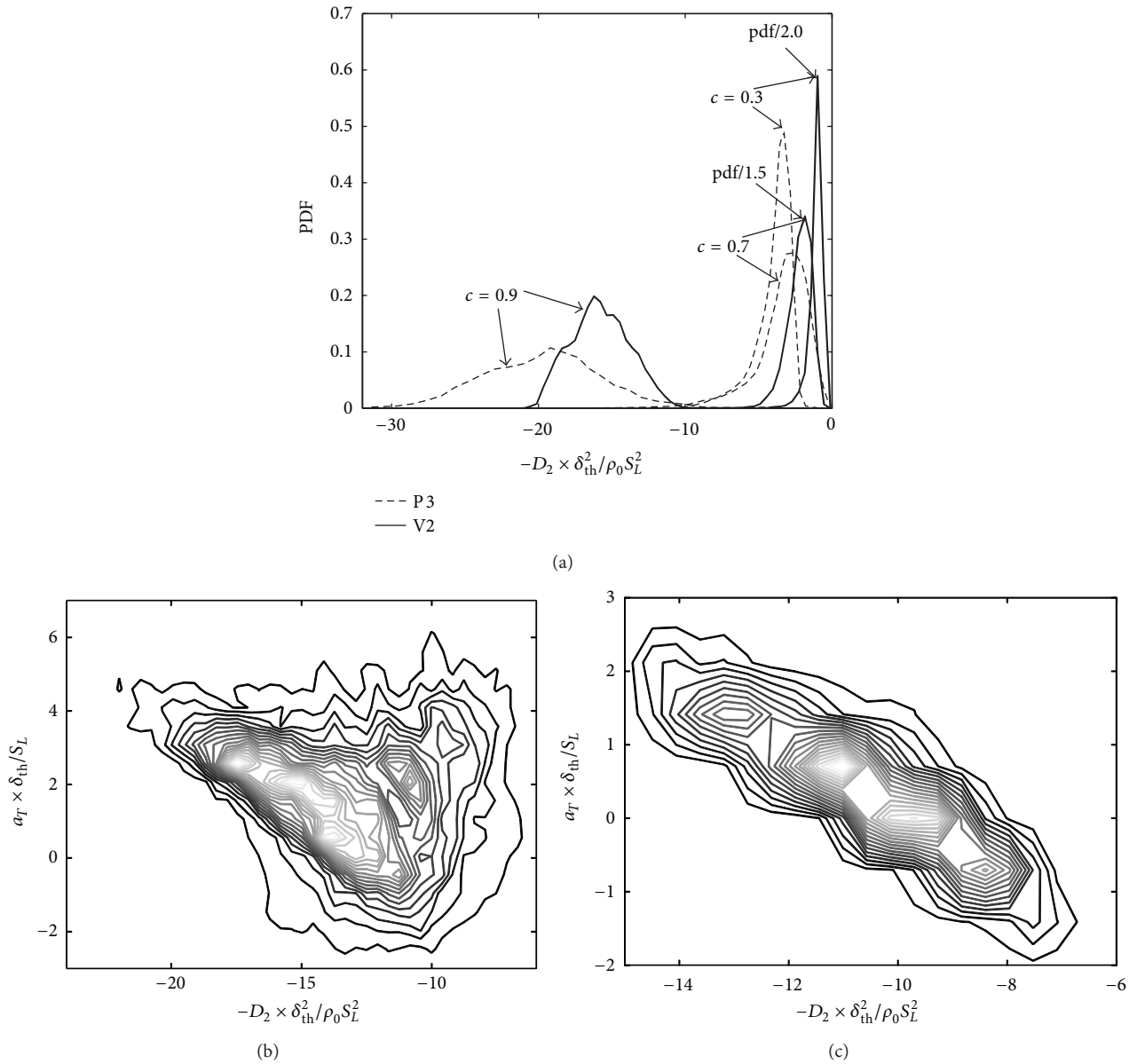

Figure 11: The marginal pdfs of $(-D_2) \times \delta_{th}^2/\rho_0 S_L^2$ for $c = 0.3$, 0.7, and 0.9 for cases (a) P3 and V2. Joint pdfs between $(-D_2) \times \delta_{th}^2/\rho_0 S_L^2$ and normalised tangential strain rate $a_T \times \delta_{th}/S_L$ on $c = 0.8$ isosurface for cases (b) P3 and (c) V2.

Table 3: Correlation coefficients between $(-D_2)$ and a_T and between $(-D_2)$ and κ_m on $c = 0.1$, 0.3, 0.5, 0.7, and 0.9 isosurfaces.

Case	$(-D_2) - a_T$					$(-D_2) - \kappa_m$				
	$c = 0.1$	$c = 0.3$	$c = 0.5$	$c = 0.7$	$c = 0.9$	$c = 0.1$	$c = 0.3$	$c = 0.5$	$c = 0.7$	$c = 0.9$
P1	−0.598	−0.809	−0.368	−0.183	−0.522	0.280	0.577	0.582	−0.020	0.261
P2	−0.581	−0.806	−0.389	−0.218	−0.488	0.272	0.554	0.600	0.023	0.225
P3	−0.546	−0.699	−0.028	0.050	−0.296	0.283	0.422	0.364	−0.234	−0.001
P4	−0.513	−0.652	0.221	−0.078	−0.483	0.231	0.338	−0.074	−0.412	−0.100
P5	−0.472	−0.581	0.111	−0.031	−0.378	0.205	0.288	0.174	−0.317	−0.107
V1	−0.712	−0.695	−0.069	−0.616	−0.679	0.700	0.825	−0.176	0.619	0.766
V2	−0.628	−0.525	0.089	−0.445	−0.703	0.475	0.696	0.033	0.159	0.633
V3	−0.452	−0.355	0.130	−0.312	−0.697	0.289	0.481	0.049	−0.104	0.260

only existent within the flame thickness. Alternatively, $(-D_2)$ can be considered to be governed by small-scale eddies and thus the characteristic length scale can be taken to be the Kolmogorov length scale η. Thus one obtains $(-D_2) \sim (-\rho D^2/\eta^4) \sim (-\rho N_c^2)\mathrm{Ka}^2$ when dissipation processes are taken to be governed by η but $\delta/\eta \sim \mathrm{Ka}^{1/2}$ remains of the order of unity for all cases considered here (see Table 1) and both scalings of $(-D_2)$ (i.e., $(-D_2) \sim (-\rho D^2/\delta^4) \sim (-\rho N_c^2)$ and $(-D_2) \sim (-\rho D^2/\eta^4) \sim (-\rho N_c^2)\mathrm{Ka}^2$) suggest that high magnitudes of the dissipation term $|-D_2|$ are associated with high values of a_T due to positive correlation between N_c and a_T (see Figure 5(a)).

(ii) As $(-D_2)$ assumes negative values, the quantities $(-D_2)$ and a_T are predominantly negatively correlated throughout the flame due to positive correlation between $|-D_2|$ and a_T. However, the negative correlation between $(-D_2)$ and a_T weakens with increasing u'/S_L due to weakening of positive correlation between N_c and a_T. Thus the correlation between $(-D_2)$ and a_T becomes weakly positive at the middle of the flame for high values of u'/S_L (e.g., cases P4 and P5).

The joint pdfs of $(-D_2)$ and curvature κ_m for cases P3 and V2 are shown in Figure 12 for $c = 0.3$, 0.7, and 0.9 isosurfaces and the correlation coefficients between $(-D_2)$ and κ_m for different c isosurfaces across the flame are shown in Table 3 for all cases considered here. The joint pdfs of $(-D_2)$ and κ_m in cases P1, P2, P4, and P5 (cases V1 and V3) are qualitatively similar to those in case P3 (case V2) and thus are not shown here. It can be seen from Figure 12 that the quantities $(-D_2)$ and κ_m are nonlinearly related to one another. The physical explanations behind the observed behaviour are provided below.

(i) The molecular dissipation term $(-D_2)$ can alternatively be expressed as

$$\begin{aligned}(-D_2) &= -2\rho D^2 \left\{ \begin{array}{l} \left[\dfrac{\partial|\nabla c|}{\partial n}\right]^2 + 4\kappa_m|\nabla c|\dfrac{\partial|\nabla c|}{\partial n} + 4\kappa_m^2|\nabla c|^2 \\ +2\left[\dfrac{\partial^2 c}{\partial x_1\partial x_2}\dfrac{\partial^2 c}{\partial x_1\partial x_2} - \dfrac{\partial^2 c}{\partial x_1\partial x_1}\dfrac{\partial^2 c}{\partial x_2\partial x_2}\right] \\ +2\left[\dfrac{\partial^2 c}{\partial x_1\partial x_3}\dfrac{\partial^2 c}{\partial x_1\partial x_3} - \dfrac{\partial^2 c}{\partial x_1\partial x_1}\dfrac{\partial^2 c}{\partial x_3\partial x_3}\right] \\ +2\left[\dfrac{\partial^2 c}{\partial x_2\partial x_3}\dfrac{\partial^2 c}{\partial x_2\partial x_3} - \dfrac{\partial^2 c}{\partial x_2\partial x_2}\dfrac{\partial^2 c}{\partial x_3\partial x_3}\right] \end{array} \right\}. \\ &\qquad (8)\end{aligned}$$

The above expression clearly indicates that the third term on the right hand side of (8) (i.e., $-8\rho D^2\kappa_m^2|\nabla c|^2$) induces nonlinear curvature dependence of the molecular dissipation term $(-D_2)$.

(ii) The quantity $\partial|\nabla c|/\partial n$ remains negative (positive) towards the unburned (burned) gas side of the flame [10, 59, 60]; thus the second term on the right hand side is positively (negatively) correlated with κ_m towards the unburned (burned) gas side of the flame. The first term on the right hand side of (8) can be taken to scale with $(-\rho N_c^2)$ (i.e., $-2\rho D^2(\partial|\nabla c|/\partial n)^2 \sim -2\rho N_c^2$). It has already been shown that the joint pdfs of N_c and κ_m exhibit both positive and negative correlating branches for high values of u'/S_L (see cases P5 and V3 in Figure 5(b)) and thus the joint pdf of $-2\rho D^2(\partial|\nabla c|/\partial n)^2$ and κ_m is also expected to show branches with both positive and negative correlations in these cases. The weak negative correlation between N_c and κ_m for small values of u'/S_L (see cases P1 and V1 in Figure 5(b)) leads to weak positive correlation between $-2\rho D^2(\partial|\nabla c|/\partial n)^2 \sim -2\rho N_c^2$ and κ_m. The last three terms on the right hand side vanish in the limit of small scale isotropy and for the present cases they remain weakly correlated with curvature.

The relative strengths of the above mechanisms determine the net curvature dependence of $(-D_2)$. Thus, both positive and negative correlations between $(-D_2)$ and κ_m have been observed within the flame front in all cases considered here.

3.8. Local Behaviour of $f(D)$ and Its Curvature and Strain Rate Dependences. The marginal pdfs of $f(D)$ for $c = 0.1$, 0.3, 0.5, 0.7, and 0.9 isosurfaces across the flame front are shown in Figure 13(a) for cases P3 and V2. The pdfs of $f(D)$ in cases P1, P2, P4, and P5 (cases V1 and V3) are qualitatively similar to those in case P3 (case V2) and thus are not explicitly shown here. It is evident from Figure 13(a) that $f(D)$ predominantly assumes negative (positive) values towards the unburned (burned) gas side of the flame (see Figure 3). The density-weighted diffusivity ρD is considered to be constant in cases P1–P5 and thus T_{D1} and T_{D2} are identically zero in these cases. The marginal pdfs of T_{D3} and T_{D4} for case P3 are shown in Figures 13(b) and 13(c), which show that both T_{D3} and T_{D4} predominantly assume positive (negative) values towards burned (unburned) gas side of the flame. As $T_{D5} = T_1/2$ in cases P1–P5, the pdfs of T_{D5} are qualitatively similar to those of T_1 and thus are not shown here. This indicates that T_{D5} shows predominant probability of finding positive values throughout the flame (see Figure 6). The pdfs of $T_{D1}, T_{D2}, T_{D3}, T_{D4}$, and T_{D5} for case V2 are shown in Figures 13(d)–13(h), respectively. It is evident from Figures 13(f) and 13(g) that both T_{D3} and T_{D4} assume positive (negative) values towards burned (unburned) gas side of the flame, whereas T_{D5} assumes positive values throughout the flame, which is qualitatively similar to the behaviour of the corresponding term in case P3, where ρD is assumed to be constant. Figures 13(d) and 13(e) show that both T_{D1} and T_{D2} assume predominantly positive (negative) values towards the unburned (burned) gas side of the flame.

The contours of joint pdfs between $f(D)$ and a_T (κ_m) for $c = 0.1$, 0.5, and 0.7 isosurfaces are shown in Figure 14 (Figure 15) for cases P3 and V2, and the correlation coefficients between $f(D)$ and a_T (κ_m) for different c isosurfaces across the flame for cases P3 and V2 are shown in Figures 16(a) and 16(b) (Figures 16(c) and 16(d)), respectively.

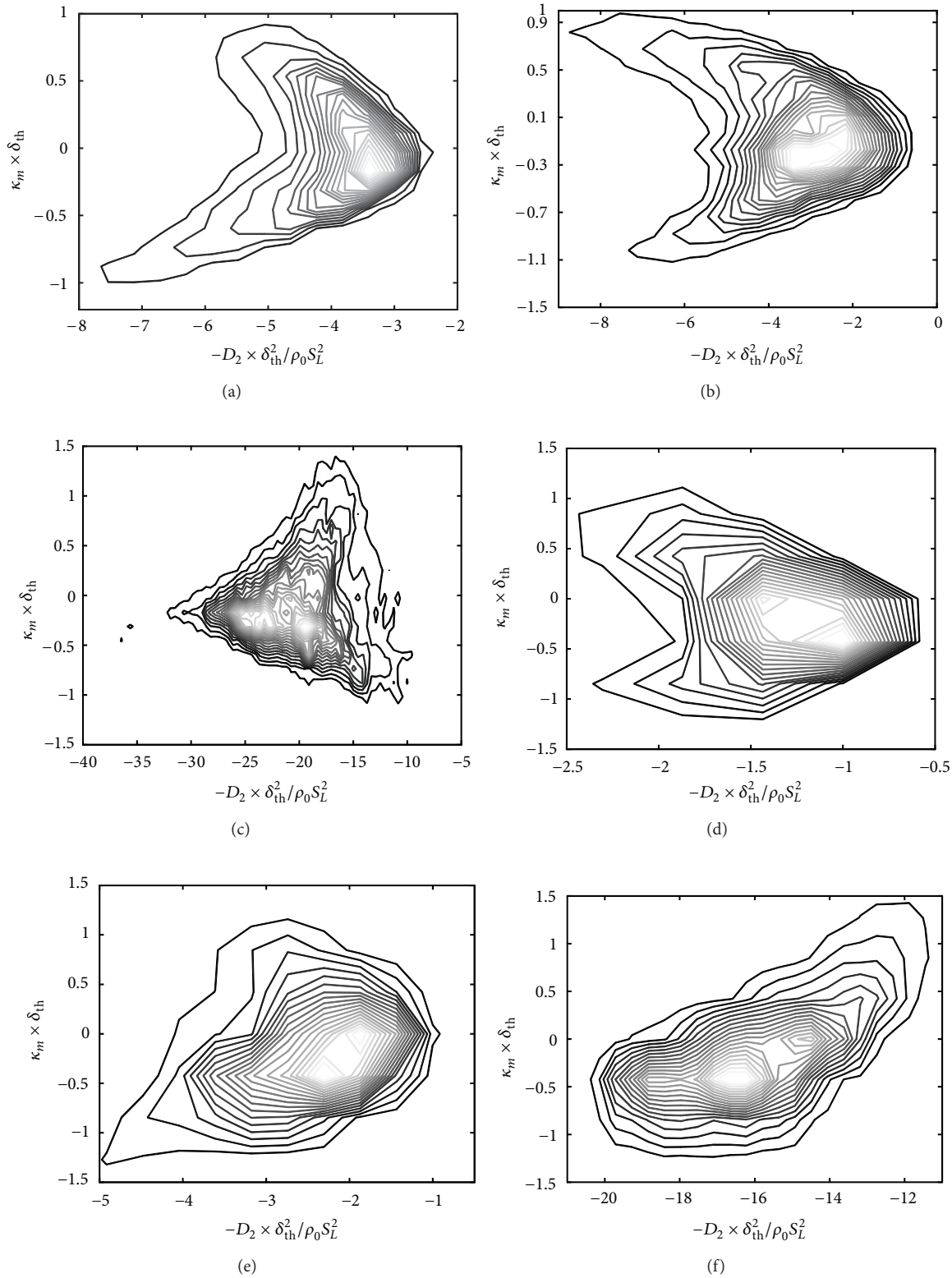

FIGURE 12: Joint pdfs between $(-D_2) \times \delta_{th}^2/\rho_0 S_L^2$ and normalised curvature $\kappa_m \times \delta_{th}$ on (a) $c = 0.3$, (b) 0.7. and (c) 0.9 isosurfaces for case P3. Joint pdfs between $(-D_2) \times \delta_{th}^2/\rho_0 S_L^2$ and normalised curvature $\kappa_m \times \delta_{th}$ on (d) $c = 0.3$, (e) 0.7, and (f) 0.9 isosurfaces for case V2.

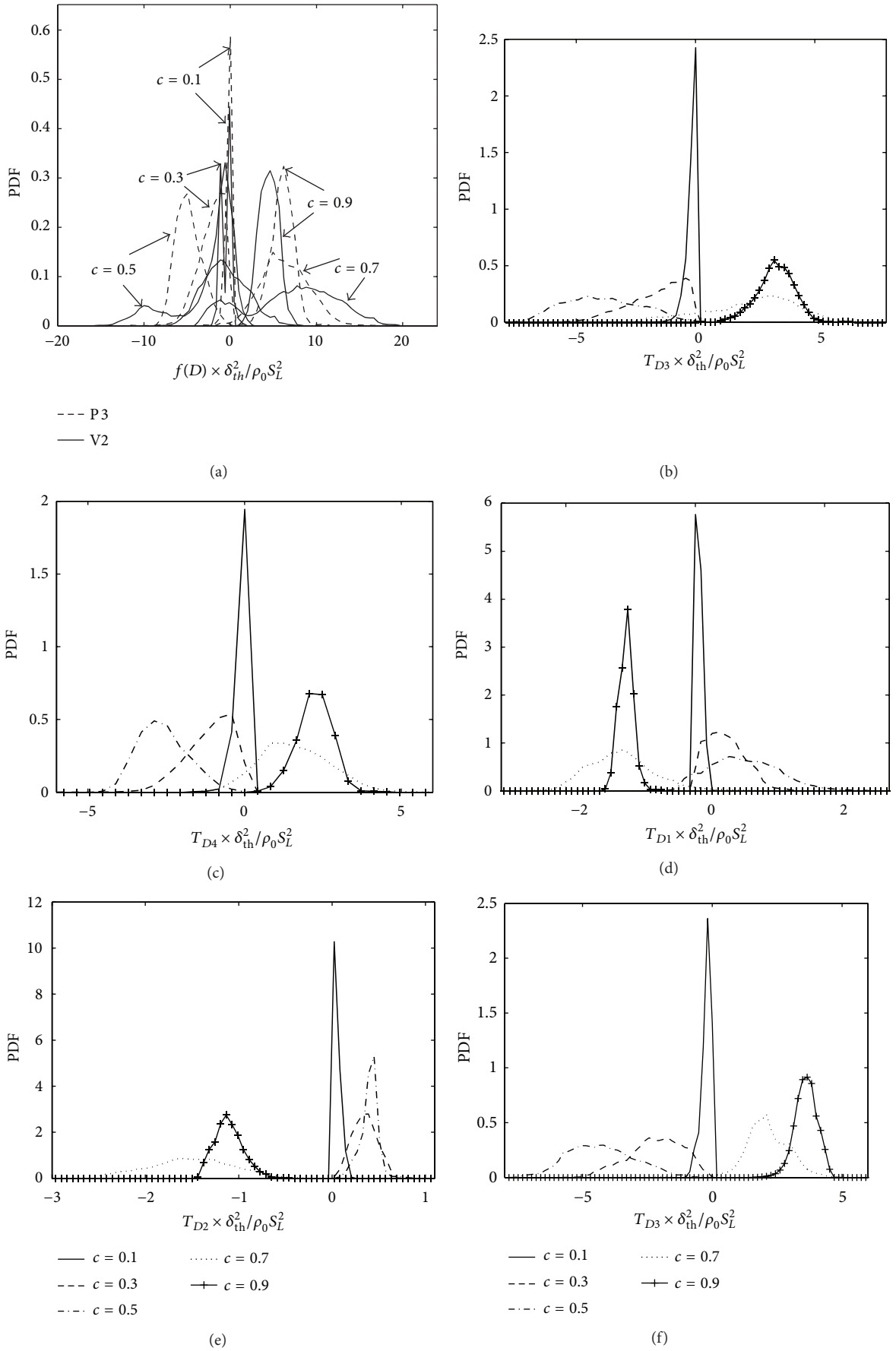

Figure 13: Continued.

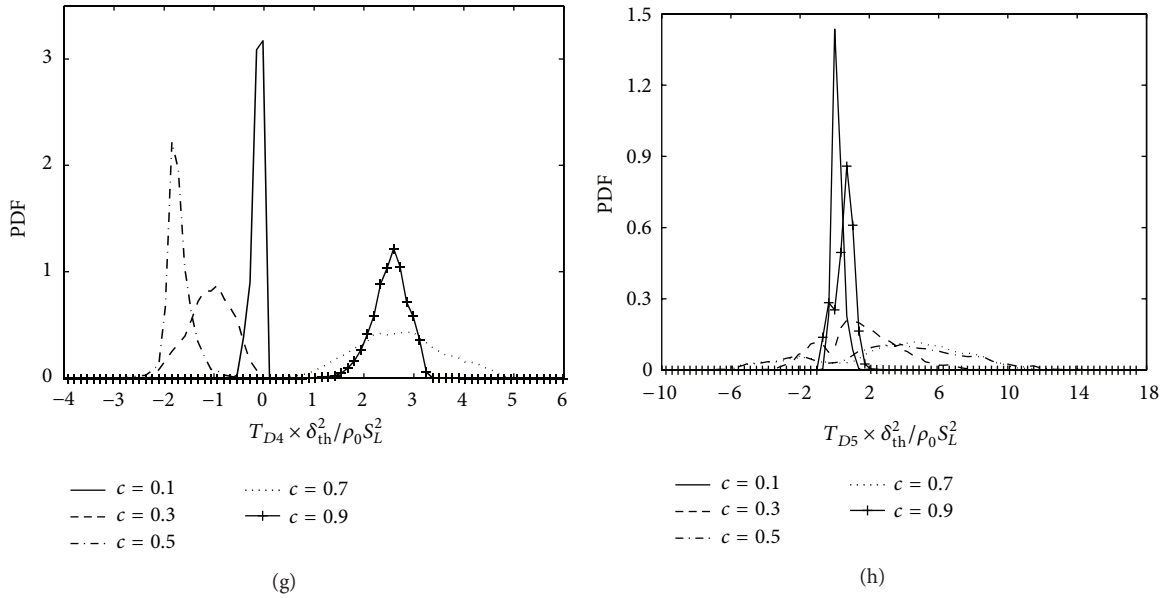

FIGURE 13: The marginal pdfs of $f(D)\times\delta_{th}^2/\rho_0 S_L^2$ for c = 0.1, 0.3, 0.5, 0.7, and 0.9 for cases (a) P3 and V2. The marginal pdfs of (b) $T_{D3}\times\delta_{th}^2/\rho_0 S_L^2$ and (c) $T_{D4}\times\delta_{th}^2/\rho_0 S_L^2$ for c = 0.1, 0.3, 0.5, 0.7, and 0.9 across the flame for case P3. The marginal pdfs of (d) $T_{D1}\times\delta_{th}^2/\rho_0 S_L^2$, (e) $T_{D2}\times\delta_{th}^2/\rho_0 S_L^2$, (f) $T_{D3}\times\delta_{th}^2/\rho_0 S_L^2$, (g) $T_{D4}\times\delta_{th}^2/\rho_0 S_L^2$, and (h) $T_{D5}\times\delta_{th}^2/\rho_0 S_L^2$ for c = 0.1, 0.3, 0.5, 0.7, and 0.9 across the flame for case V2.

Both Figures 14 and 16 indicate that $f(D)$ and a_T are negatively (positively) correlated with each other towards the unburned (burned) gas side of the statistically planar flame (i.e., case P3), whereas $f(D)$ and a_T are positively correlated with each other from the middle to the burned gas side in the V-flame case (i.e., case V2), but this correlation remains weak towards the unburned gas side. It is evident from Figure 15 that $f(D)$ and κ_m remain weakly correlated for both statistically planar and V-flames, which is consistent with the correlation coefficient between $f(D)$ and κ_m shown in Figures 16(c) and 16(d). However, there are qualitative differences in the joints pdfs between $f(D)$ and κ_m for cases P3 and V2.

In order to explain the observed strain rate dependence of $f(D)$, the correlation coefficients between T_{D3}, T_{D4}, and T_{D5} ($T_{D1}, T_{D2}, T_{D3}, T_{D4}$, and T_{D5}) with a_T, for c = 0.1, 0.3, 0.5, 0.7, and 0.9 isosurfaces, are also shown in Figure 16(a) (Figure 16(b)) for case P3 (case V2). It is evident from Figures 16(a) and 16(b) that both T_{D3} and T_{D4} remain negatively (positively) correlated with a_T towards the unburned (burned) gas side of the flame.

The strain rate dependences of $T_{D1}, T_{D2}, T_{D3}, T_{D4}$, and T_{D5} can be explained in the following manner.

(i) The magnitudes of T_{D3} and T_{D4} can be taken to scale as $|T_{D3}| \sim \rho D N_c/\delta^2 \sim \rho N_c^2$ and $|T_{D4}| \sim \rho D N_c/\delta^2 \sim \rho N_c^2$, which indicates that $|T_{D3}| \sim \rho N_c^2$ and $|T_{D4}| \sim \rho N_c^2$ remain positively correlated with a_T due to positive correlation between N_c and a_T (see Figure 5(a)). This suggests that the negative (positive) values of T_{D3} and T_{D4} (see Figures 13, 16(a), and 16(b)) lead to negative (positive) correlations of these terms with a_T due to positive correlations between N_c and a_T (also due to positive correlation between $|T_{D3}| \sim \rho N_c^2$ ($|T_{D4}| \sim \rho N_c^2$) and a_T).

(ii) The term T_{D5} remains positively correlated with a_T throughout the flame, which is consistent with the positive correlation between T_1 and a_T shown in Figure 6(c), as $T_{D5} = 0.5T_1$ in statistically planar cases P1–P5 considered here (see Figure 16(a)). Even though ρD increases with increasing temperature in cases V1–V3, T_{D5} can still be taken to scale with T_1 (i.e., $T_{D5} \sim T_1 \sim \rho\tau N_c S_L/\delta$) and the positive correlation between T_1 and a_T leads to a positive correlation between T_{D5} and a_T in case V2 and also in cases V1 and V3 (see Figure 16(b)).

(iii) The magnitudes of the terms T_{D1} and T_{D2} can be scaled as $|T_{D1}| \sim \rho D^2/\delta^4 \sim \rho N_c^2$ and $|T_{D2}| \sim \rho D^2/\delta^4 \sim \rho N_c^2$, respectively, which suggests that $|T_{D1}|$ and $|T_{D2}|$ are expected to be positively correlated with a_T due to positive correlation between N_c and a_T (see Figure 5(a)). As T_{D1} and T_{D2} assume predominantly positive (negative) values towards the unburned (burned) gas side of the flame, these terms scale with $T_{D1} \sim T_{D2} \sim \rho N_c^2$ ($T_{D1} \sim T_{D2} \sim -\rho N_c^2$) towards the reactant (product) side of the flame. Thus the positive correlation between N_c and a_T leads to positive (negative) $T_{D1} - a_T$ and $T_{D2} - a_T$ correlations towards the unburned (burned) gas side of the flame (see Figure 16(b)).

(iv) In cases P1–P5, the terms T_{D3}, T_{D4}, and T_{D5} remain positively correlated with a_T towards the burned gas side of the flame (see Figure 16(a)) and these positive correlations result in a net positive correlation between $f(D)$ and a_T towards the burned gas

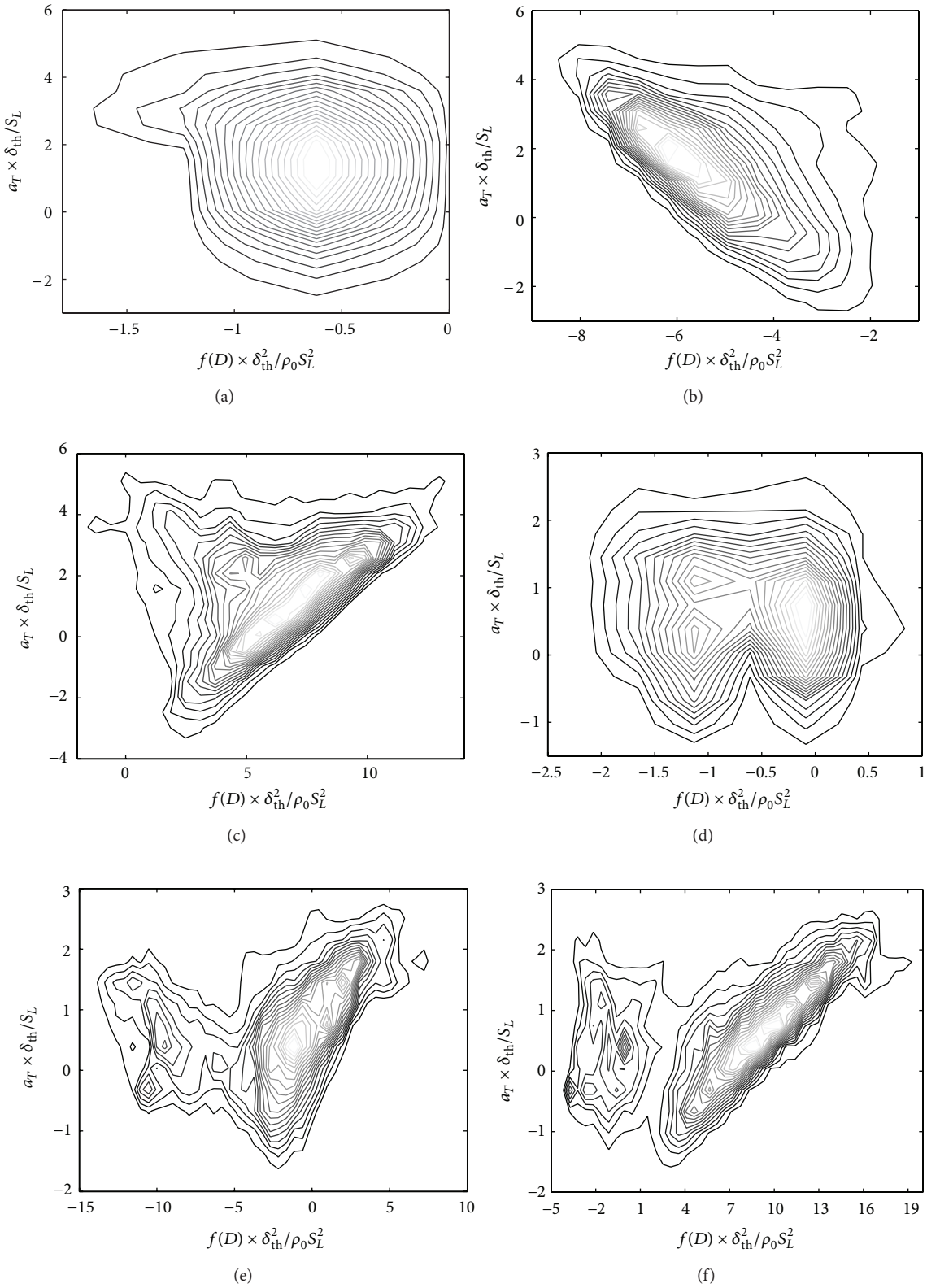

FIGURE 14: Joint pdfs between $f(D) \times \delta_{th}^2/\rho_0 S_L^2$ and normalised tangential strain rate $a_T \times \delta_{th}/S_L$ for case P3 on (a) $c = 0.1$, (b) 0.5, and (c) 0.7 isosurfaces. Joint pdfs between $f(D) \times \delta_{th}^2/\rho_0 S_L^2$ and normalised tangential strain rate $a_T \times \delta_{th}/S_L$ for case V2 on (d) $c = 0.1$, (e) 0.5, and (f) 0.7 isosurfaces.

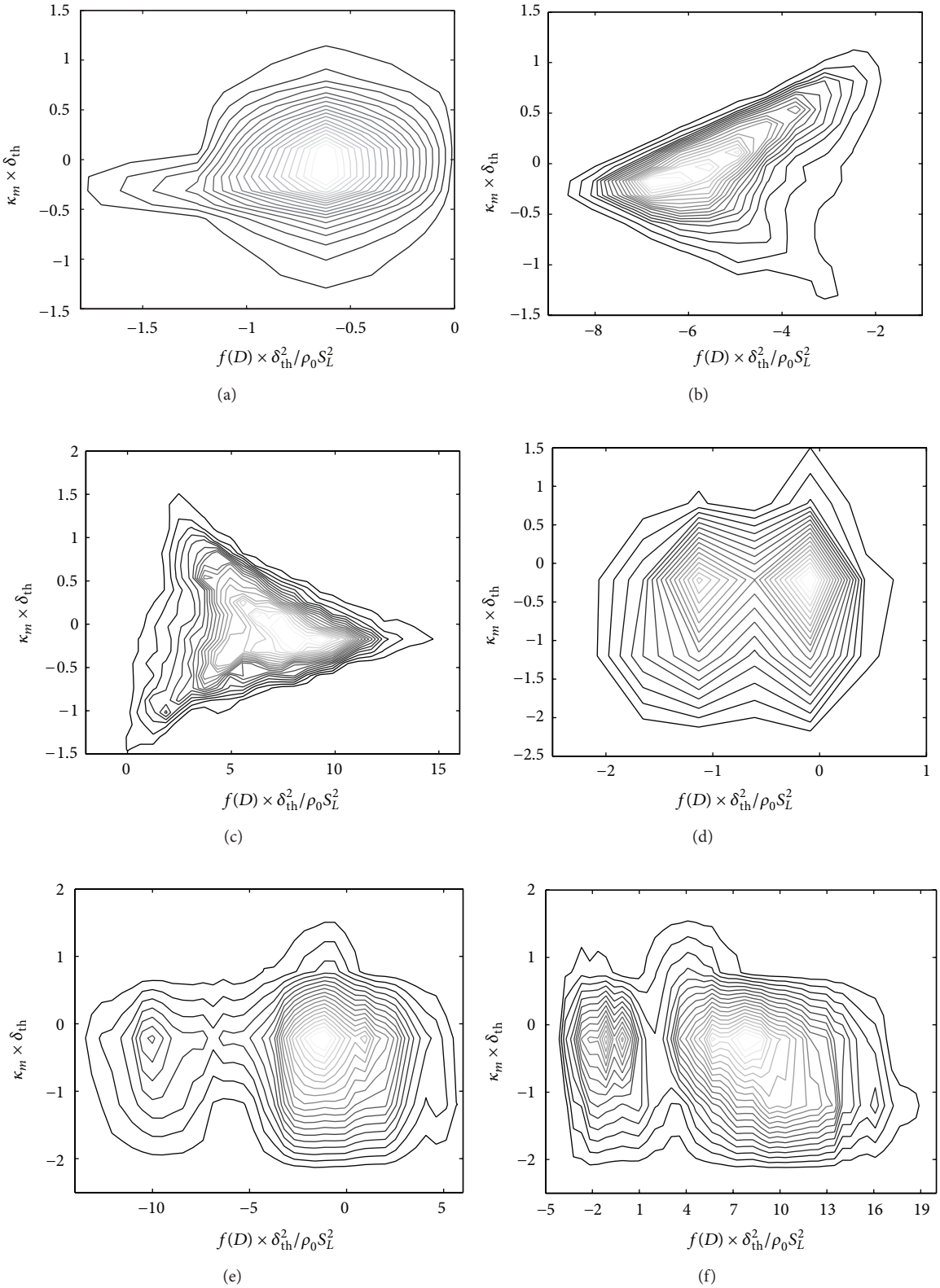

FIGURE 15: Joint pdfs between $f(D) \times \delta_{th}^2/\rho_0 S_L^2$ and normalised curvature $\kappa_m \times \delta_{th}$ on (a) $c = 0.1$, (b) 0.5, and (c) 0.7 isosurfaces for case P3. Joint pdfs between $f(D) \times \delta_{th}^2/\rho_0 S_L^2$ and normalised curvature $\kappa_m \times \delta_{th}$ on (d) $c = 0.1$, (e) 0.5, and (f) 0.7 isosurfaces for case V2.

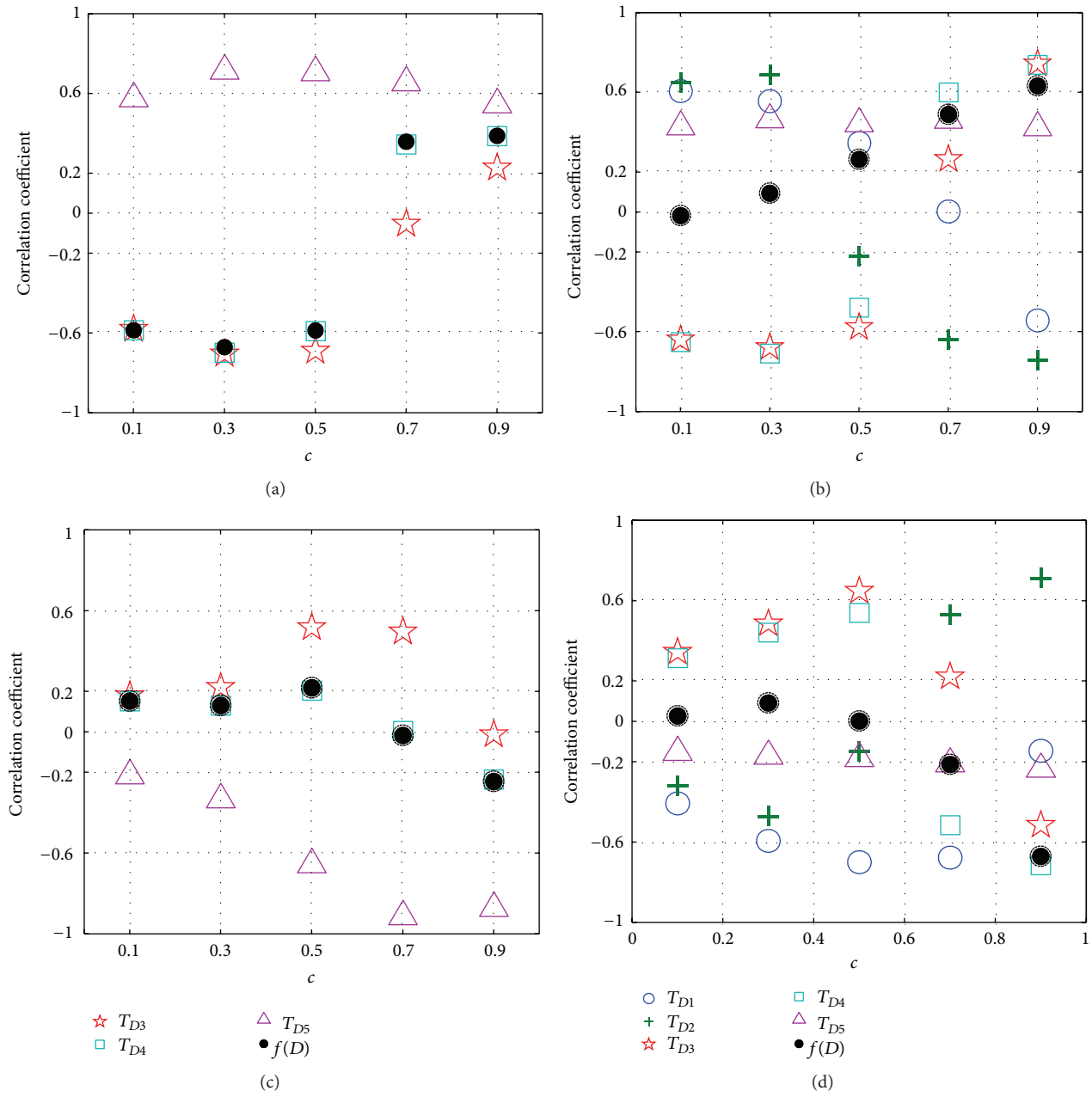

FIGURE 16: (a) Correlation coefficients for the $T_{D3} - a_T$, $T_{D4} - a_T$, $T_{D5} - a_T$, and $f(D) - a_T$ correlations on $c = 0.1$, 0.3, 0.5, 0.7, and 0.9 isosurfaces for case P3. (b) Correlation coefficients for the $T_{D1} - a_T$, $T_{D2} - a_T$, $T_{D3} - a_T$, $T_{D4} - a_T$, $T_{D5} - a_T$, and $f(D) - a_T$ correlations on $c = 0.1$, 0.3, 0.5, 0.7, and 0.9 isosurfaces for case V2. (c) Correlation coefficients for the $T_{D3} - \kappa_m$, $T_{D4} - \kappa_m$, $T_{D5} - \kappa_m$, and $f(D) - \kappa_m$ correlations on $c = 0.1$, 0.3, 0.5, 0.7, and 0.9 isosurfaces for case P3. (d) Correlation coefficients for the $T_{D1} - \kappa_m$, $T_{D2} - \kappa_m$, $T_{D3} - \kappa_m$, $T_{D4} - \kappa_m$, $T_{D5} - \kappa_m$, and $f(D) - \kappa_m$ correlations on $c = 0.1$, 0.3, 0.5, 0.7, and 0.9 isosurfaces for case V2.

side of the flame. On the other hand, T_{D3} and T_{D4} remain negatively correlated with a_T towards the unburned gas side of the flame (see Figure 16(a)) and these correlations dominate over the positive correlation between T_{D5} and a_T to result in a net negative correlation between $f(D)$ and a_T towards the unburned gas side of the flame.

(v) In cases V1–V3, the terms T_{D3}, T_{D4}, and T_{D5} remain positively correlated with a_T towards the burned gas side of the flame (see Figure 16(b)) and these positive correlations overcome the negative $T_{D1} - a_T$ and $T_{D2} - a_T$ correlations to give rise to a net positive correlation between $f(D)$ and a_T towards the burned gas side of the flame. By contrast, T_{D3} and T_{D4} remain negatively correlated with a_T towards the unburned gas side of the flame (see Figure 16(b)) and these correlations oppose the positive $T_{D1} - a_T$, $T_{D2} - a_T$, and $T_{D5} - a_T$ correlations to result in a weak correlation between

$f(D)$ and a_T towards the unburned gas side of the flame.

The correlation coefficients between T_{D3}, T_{D4}, and T_{D5} ($T_{D1}, T_{D2}, T_{D3}, T_{D4}$, and T_{D5}) with κ_m for $c = 0.1$, 0.3, 0.5, 0.7, and 0.9 isosurfaces are also shown in Figure 16(c) (Figure 16(d)) for case P3 (case V2). It is evident from Figures 16(c) and 16(d) that $f(D)$ and κ_m are weakly correlated throughout the flame for both planar and V-flame cases. The curvature κ_m dependences of $T_{D1}, T_{D2}, T_{D3}, T_{D4}, T_{D5}$, and $f(D)$ can be explained in the following manner.

(i) Both T_{D3} and T_{D4} remain negatively (positively) correlated with a_T towards the unburned (burned) gas side of the flame for both planar and V-flame cases (see Figures 16(a) and 16(b)), whereas a_T and κ_m are negatively correlated throughout the flame. Thus, high (low) values of T_{D3} and T_{D4} are associated with high positive values of κ_m towards the unburned (burned) gas side of the flame, which gives rise to positive (negative) correlations of T_{D3} and T_{D4} with κ_m towards the unburned (burned) gas side.

(ii) As $T_{D5} = 0.5T_1$ for statistically planar flame cases (i.e., case P1–P5), a strong negative correlation between T_{D5} and κ_m has been observed near $c = 0.7$ isosurface, which is consistent with the negative correlation between T_1 and κ_m shown in Figure 6(e). Even though ρD increases with increasing temperature in V-flame cases (i.e., cases V1–V3), T_{D5} can still be taken to scale with T_1 (i.e., $T_{D5} \sim T_1 \sim \rho\tau N_c S_L/\delta$) and the negative correlation between T_1 and κ_m (see Figure 6(f)) leads to a weak negative correlation between T_{D5} and κ_m in case V2 and also in cases V1 and V3.

(iii) Both T_{D1} and T_{D2} remain positively (negatively) correlated with a_T towards the unburned (burned) gas side of the flame in case V2 (see Figure 16(b)), whereas a_T and κ_m are negatively correlated throughout the flame. Thus, small (high) values of T_{D1} and T_{D2} are associated with high positive (negative) values of κ_m towards the unburned gas side of the flame, which gives rise to negative correlations of T_{D1} and T_{D2} with κ_m towards the unburned gas side in case V2. The combination of negative correlations of T_{D1} and T_{D2} with a_T towards the burned gas side, as well as the strengthening of negative correlation between a_T and κ_m towards the burned gas side of the flame, leads to the weakening of negative correlations of T_{D1} and T_{D2} with κ_m, as the burned gas side is approached and the correlation between T_{D2} with κ_m eventually becomes positive towards the burned gas side of the flame (see Figure 16(d)).

(iv) The terms T_{D3}, T_{D4}, and T_{D5} remain negatively correlated with κ_m towards the burned gas side of the flame and these negative correlations dominate over weak positive $T_{D1} - \kappa_m$ and $T_{D2} - \kappa_m$ correlations to result in a net negative correlation between $f(D)$ and κ_m towards the burned gas side of the flame in case V2. The terms T_{D3} and T_{D4} remain positively correlated with κ_m towards the unburned gas side of the flame (see Figure 16(d)) and these correlations are opposed by the negative $T_{D1} - \kappa_m$, $T_{D2} - \kappa_m$, and $T_{D5} - \kappa_m$ correlations to result in a weak correlation between $f(D)$ and κ_m towards the unburned gas side of the flame front in case V2 and other V-flame cases.

3.9. Modelling Significances. A modelled transport equation of $\widetilde{N}_c$ may need to be solved alongside other modelled conservation equations in RANS/LES simulations, when the rate of generation of scalar gradients does not remain in equilibrium with its destruction rate. The local strain rate and curvature dependences of SDR are expected to play important roles in LES simulations, as the necessity of capturing local behaviour of $\widetilde{N}_c$ is particularly important in the context of LES. As $\widetilde{N}_c$ approaches N_c with decreasing filter width Δ (i.e., $\lim_{\Delta \to 0} \widetilde{N}_c = N_c$) in the context of LES, the local resolved-scale strain rate and curvature dependences of $\widetilde{N}_c$ and the terms of its transport equation (i.e., $\overline{T}_1, \overline{T}_2, \overline{T}_3, (-\overline{D}_2)$, and $\overline{f(D)}$) are likely to be qualitatively similar to the local strain rate and curvature dependences of N_c and the terms of its transport equation (i.e., $T_1, T_2, T_3, (-D_2)$, and $f(D)$), respectively. The above discussion suggests that the models for $\widetilde{N}_c, \overline{T}_1, \overline{T}_2, \overline{T}_3, (-\overline{D}_2)$, and $\overline{f(D)}$ in LES should be developed in such a manner so that they are capable of capturing the resolved strain rate and curvature dependences of $\widetilde{N}_c, \overline{T}_1, \overline{T}_2, \overline{T}_3, (-\overline{D}_2)$, and $\overline{f(D)}$ for a range of different filter widths and approach local strain rate and curvature dependences of $N_c, T_1, T_2, T_3, (-D_2)$, and $f(D)$ for small filter widths.

It can further be observed from Figures 5–16 that the local strain rate and curvature dependence of N_c and the terms of its transport equation for V-flames are found to be qualitatively similar to the behaviour observed for the statistically planar flame cases. As the SDR statistics are principally governed by the small-scale molecular processes, the local statistics of N_c and the terms of its transport equation are largely independent of the flow configuration. Thus, the models for $\widetilde{N}_c$ transport developed based on data extracted from a canonical configuration might broadly be applicable to different geometries.

Moreover, it is worth noting that ρD is assumed to be constant in cases P1–P5 whereas ρD is taken to be temperature dependent in cases V1–V3. However, the statistical behaviours of N_c and the terms of its transport equation are found to be broadly similar qualitatively in all cases indicating that the models, which have been developed based on DNS databases with constant ρD, should at least be able to capture the qualitative trends of $\widetilde{N}_c$ transport.

4. Conclusions

The statistical behaviours of the instantaneous SDR N_c and the terms of its transport equation have been analysed using simple chemistry DNS databases of statistically planar and V-flames for a range of different values of turbulent Reynolds number. It has been found that the mean and local behaviours of N_c and the terms of its transport equation are similar

for both statistically planar and V-flames for the range of turbulent Reynolds number explored here. In all the cases, N_c is positively correlated with tangential strain rate a_T throughout the flame. By contrast, N_c and local curvature κ_m remain negatively correlated for small values of u'/S_L but the joint pdf of N_c and κ_m shows branches with both positive and negative correlation, and the net correlation becomes weak for high values of u'/S_L. It has been found that the mean contributions of the density-variation term T_1 and the molecular dissipation term $(-D_2)$ in the transport equation of N_c are the leading order source and sink, respectively. The mean value of the strain rate contribution T_2 to the SDR transport is predominantly negative for the major part of the flame due to predominant ∇c alignment with the most extensive principal strain rate e_α, although positive contributions of T_2 were observed towards the unburned gas side for high u'/S_L cases where ∇c preferentially aligns with the most compressive principal strain rate e_γ. The mean value of the reaction rate contribution to the SDR transport T_3 remains positive for the major part of the flame before assuming negative values towards the burned gas side. The mean contribution of the term originating due to the diffusivity gradient in the SDR transport $f(D)$ remains negative towards the unburned gas side before assuming positive values towards the burned gas side of the flame.

It has been found that the density variation term T_1 remains positively correlated with tangential strain rate a_T, whereas the correlation between T_1 and the local curvature κ_m is negative throughout the flame. The strain rate term T_2 is predominantly positively correlated with both a_T and κ_m for the major part of the flame front. The qualitative nature of the local strain rate and curvature dependences of T_3, $(-D_2)$, and $f(D)$ change across the flame. The reaction rate contribution T_3 and the tangential strain rate a_T remain positively (negatively) correlated towards the unburned (burned) gas side of the flame. However, T_3 is weakly correlated with curvature κ_m throughout the flame for all cases considered here. The molecular dissipation term $(-D_2)$ is negatively correlated with a_T throughout the flame, whereas the joint pdf of $(-D_2)$ and κ_m shows branches with both positive and negative correlation and their qualitative behaviours change across the flame. The diffusivity gradient term $f(D)$ and a_T are found to be negatively (positively) correlated with each other towards the unburned (burned) gas side of the flame, whereas the joint pdfs of $f(D)$ and κ_m show a weak positive (negative) correlation in the unburned (burned) gas side of the flame. Detailed physical explanations have been provided for the strain rate and curvature dependences of N_c and the terms of its transport equation. The qualitative nature of these statistics has been found to be unaltered for the range of turbulent Reynolds number Re_t considered here, but the strength of the correlations is affected by Re_t. Moreover, the local strain rate and curvature dependence of N_c and the terms of its transport equation for V-flames are found to be broadly similar qualitatively to the behaviour observed for the statistically planar flame cases. Moreover, the assumption of mass diffusivity variation with temperature has been shown not to affect the qualitative behaviour of SDR and its transport statistics.

In the context of single step chemistry, the reaction progress variable c can be uniquely defined, but c can be defined based on different species mass fractions in the presence of detailed chemistry. However, the conclusions drawn in this analysis are unlikely to change if c is defined based on the mass fraction of a major reactant/product, which is closely correlated with density change and heat release. The present single-step Arrhenius type chemistry qualitatively captures the statistics of $|\nabla c|$ transport obtained using detailed chemistry based simulations for the flames with global Lewis number close to unity. This can be substantiated by qualitative similarities between the strain rate and curvature dependence of the terms of $|\nabla c|$ transport equation obtained from detailed chemistry [14] and single-step chemistry [15] based DNS simulations. Given the close relation between $|\nabla c|$ and SDR, it can be expected that the conclusions drawn regarding SDR transport will at least be qualitatively valid for detailed chemistry based simulations.

It is worth noting that the effects of differential diffusion of heat and mass are not addressed in the present analysis, and the presence of differential diffusion may have influences on the local strain rate and curvature dependences of N_c and the different terms of its transport equation. As the SDR statistics are principally governed by the small-scale molecular processes, the local statistics of N_c and the terms of its transport equation obtained from this analysis are expected to be qualitatively similar for higher values of Re_t than the values of turbulent Reynolds number considered here. However, this analysis has been carried out for moderate values of Re_t; thus further experimental and computational studies at large values of Re_t in the presence of detailed chemistry are needed for further confirmation and deeper understanding of the statistics of SDR transport in turbulent premixed flames.

Conflict of Interests

The authors declare that there is no conflict of interests regarding the publication of this paper.

Acknowledgment

The authors are grateful to the EPSRC, UK, for the financial support.

References

[1] R. W. Bilger, "Some aspects of scalar dissipation," *Flow, Turbulence and Combustion*, vol. 72, no. 2-4, pp. 93–114, 2004.

[2] K. N. C. Bray, "Turbulent flows with premixed reactants," in *Turbulent Reacting Flows*, P. A. Libby and F. A. Williams, Eds., pp. 115–183, Springer, New York, NY, USA, 1980.

[3] N. Chakraborty, M. Champion, A. Mura, and N. Swaminathan, "Scalar dissipation rate approach to reaction rate closure," in *Turbulent Premixed Flame*, N. Swaminathan and K. N. C. Bray, Eds., pp. 76–102, Cambridge University Press, Cambridge, UK, 1st edition, 2011.

[4] T. D. Dunstan, Y. Minamoto, N. Chakraborty, and N. Swaminathan, "Scalar dissipation rate modelling for Large Eddy

Simulation of turbulent premixed flames," *Proceedings of the Combustion Institute*, vol. 34, pp. 11193–11201, 2013.

[5] N. Peters, P. Terhoeven, J. H. Chen, and T. Echekki, "Statistics of flame displacement speeds from computations of 2-D unsteady methane-air flames," *Proceedings of the Combustion Institute*, vol. 27, pp. 833–839, 1998.

[6] J. H. Chen and H. G. Im, "Correlation of flame speed with stretch in turbulent premixed methane/air flames," *Proceedings of the Combustion Institute*, vol. 27, pp. 819–826, 1998.

[7] T. Echekki and J. H. Chen, "Analysis of the contribution of curvature to premixed flame propagation," *Combustion and Flame*, vol. 118, no. 1-2, pp. 308–311, 1999.

[8] J. H. Chen and H. G. Im, "Stretch effects on the burning velocity of turbulent premixed hydrogen/air flames," *Proceedings of the Combustion Institute*, vol. 28, no. 1, pp. 211–218, 2000.

[9] H. G. Im and J. H. Chen, "Preferential diffusion effects on the burning rate of interacting turbulent premixed hydrogen-air flames," *Combustion and Flame*, vol. 131, no. 3, pp. 246–258, 2002.

[10] N. Chakraborty and S. Cant, "Unsteady effects of strain rate and curvature on turbulent premixed flames in an inflow-outflow configuration," *Combustion and Flame*, vol. 137, no. 1-2, pp. 129–147, 2004.

[11] N. Chakraborty and R. S. Cant, "Effects of strain rate and curvature on surface density function transport in turbulent premixed flames in the thin reaction zones regime," *Physics of Fluids*, vol. 17, no. 6, pp. 1–15, 2005.

[12] E. R. Hawkes, J. H. Chen, E. R. Hawkes, and J. H. Chen, "Evaluation of models for flame stretch due to curvature in the thin reaction zones regime," vol. 30, pp. 647–653.

[13] N. Chakraborty and R. S. Cant, "A priori analysis of the curvature and propagation terms of the flame surface density transport equation for large eddy simulation," *Physics of Fluids*, vol. 19, no. 10, Article ID 105101, 2007.

[14] N. Chakraborty, E. R. Hawkes, J. H. Chen, and R. S. Cant, "The effects of strain rate and curvature on surface density function transport in turbulent premixed methane-air and hydrogen-air flames: a comparative study," *Combustion and Flame*, vol. 154, no. 1-2, pp. 259–280, 2008.

[15] N. Chakraborty and M. Klein, "Influence of Lewis number on the surface density function transport in the thin reaction zone regime for turbulent premixed flames," *Physics of Fluids*, vol. 20, no. 6, Article ID 065102, 2008.

[16] N. Chakraborty and M. Klein, "Effects of global flame curvature on surface density function transport in turbulent premixed flame kernels in the thin reaction zones regime," in *Proceedings of the 32nd International Symposium on Combustion*, pp. 1435–1443, August 2008.

[17] N. Swaminathan and K. N. C. Bray, "Effect of dilatation on scalar dissipation in turbulent premixed flames," *Combustion and Flame*, vol. 143, no. 4, pp. 549–565, 2005.

[18] R. Borghi and D. Dutoya, "On the scales of the fluctuations in turbulent combustion," *Symposium (International) on Combustion*, vol. 17, no. 1, pp. 235–244, 1979.

[19] T. Mantel and R. Borghi, "A new model of premixed wrinkled flame propagation based on a scalar dissipation equation," *Combustion and Flame*, vol. 96, no. 4, pp. 443–457, 1994.

[20] R. Borghi, "Turbulent premixed combustion: further discussions on the scales of fluctuations," *Combustion and Flame*, vol. 80, no. 3-4, pp. 304–312, 1990.

[21] A. Mura and R. Borghi, "Towards an extended scalar dissipation equation for turbulent premixed combustion," *Combustion and Flame*, vol. 133, no. 1-2, pp. 193–196, 2003.

[22] N. Swaminathan and R. W. Grout, "Interaction of turbulence and scalar fields in premixed flames," *Physics of Fluids*, vol. 18, no. 4, Article ID 045102, 2006.

[23] N. Chakraborty and N. Swaminathan, "Influence of the Damköhler number on turbulence-scalar interaction in premixed flames. I: physical insight," *Physics of Fluids*, vol. 19, no. 4, Article ID 045103, 2007.

[24] N. Chakraborty and N. Swaminathan, "Influence of the Damköhler number on turbulence-scalar interaction in premixed flames. II: model development," *Physics of Fluids*, vol. 19, no. 4, Article ID 045104, 2007.

[25] N. Chakraborty, J. W. Rogerson, and N. Swaminathan, "A priori assessment of closures for scalar dissipation rate transport in turbulent premixed flames using direct numerical simulation," *Physics of Fluids*, vol. 20, no. 4, Article ID 045106, 2008.

[26] A. Mura, K. Tsuboi, and T. Hasegawa, "Modelling of the correlation between velocity and reactive scalar gradients in turbulent premixed flames based on DNS data," *Combustion Theory and Modelling*, vol. 12, no. 4, pp. 671–698, 2008.

[27] A. Mura, V. Robin, M. Champion, and T. Hasegawa, "Small scale features of velocity and scalar fields in turbulent premixed flames," *Flow, Turbulence and Combustion*, vol. 82, no. 3, pp. 339–358, 2009.

[28] N. Chakraborty, J. W. Rogerson, and N. Swaminathan, "The scalar gradient alignment statistics of flame kernels and its modelling implications for turbulent premixed combustion," *Flow, Turbulence and Combustion*, vol. 85, no. 1, pp. 25–55, 2010.

[29] N. Chakraborty and N. Swaminathan, "Effects of lewis number on scalar dissipation transport and its modeling in turbulent premixed combustion," *Combustion Science and Technology*, vol. 182, no. 9, pp. 1201–1240, 2010.

[30] N. Chakraborty, M. Klein, and N. Swaminathan, "Effects of Lewis number on reactive scalar gradient alignment with local strain rate in turbulent premixed flames," *Proceedings of the Combustion Institute*, vol. 32, no. 1, pp. 1409–1417, 2009.

[31] J. H. Chen, A. Choudhary, B. de Supinski et al., "Terascale direct numerical simulations of turbulent combustion using S3D," *Computational Science and Discovery*, vol. 2, no. 1, Article ID 015001, 2009.

[32] K. W. Jenkins and R. S. Cant, "DNS of turbulent flame kernels," in *Proceedings of the 2nd AFOSR Conference on DNS and LES*, Knight and Sakell, Eds., pp. 192–202, Rutgers University, Kluwer Academic Publishers, 1999.

[33] T. J. Poinsot, "Boundary conditions for direct simulations of compressible viscous flows," *Journal of Computational Physics*, vol. 101, no. 1, pp. 104–129, 1992.

[34] A. A. Wray, "Minimal storage time advancement schemes for spectral methods," Report MS 202 A-1, NASA Ames Research Center, 1990.

[35] N. Peters, *Turbulent Combustion*, Cambridge University Press, Cambridge, UK, 2000.

[36] F. Charlette, C. Meneveau, and D. Veynante, "A power-law flame wrinkling model for LES of premixed turbulent combustion. Part I: non-dynamic formulation and initial tests," *Combustion and Flame*, vol. 131, no. 1-2, pp. 159–180, 2002.

[37] W. R. Grout, "An age extended progress variable for conditioning reaction rates," *Physics of Fluids*, vol. 19, no. 10, Article ID 105107, 2007.

[38] I. Han and K. Y. Huh, "Roles of displacement speed on evolution of flame surface density for different turbulent intensities and Lewis numbers in turbulent premixed combustion," *Combustion and Flame*, vol. 152, no. 1-2, pp. 194–205, 2008.

[39] N. Chakraborty, G. Hartung, M. Katragadda, and C. F. Kaminski, "Comparison of 2D and 3D density-weighted displacement speed statistics and implications for laser based measurements of flame displacement speed using direct numerical simulation data," *Combustion and Flame*, vol. 158, no. 7, pp. 1372–1390, 2011.

[40] T. D. Dunstan, N. Swaminathan, K. N. C. Bray, and R. S. Cant, "Geometrical properties and turbulent flame speed measurements in stationary premixed V-flames using direct numerical simulation," *Flow, Turbulence and Combustion*, vol. 87, no. 2-3, pp. 237–259, 2011.

[41] T. D. Dunstan, N. Swaminathan, and K. N. C. Bray, "Influence of flame geometry on turbulent premixed flame propagation: a DNS investigation," *Journal of Fluid Mechanics*, vol. 709, pp. 191–222, 2012.

[42] M. Boger, D. Veynante, H. Boughanem, and A. Trouve, "Direct numerical simulation analysis of flame surface density concept for large eddy simulation of turbulent premixed combustion," *Symposium (International) on Combustion*, vol. 1, pp. 917–925, 1998.

[43] N. Chakraborty and N. Swaminathan, "Reynolds number effects on scalar dissipation rate transport and its modelling in turbulent premixed combustion," *Combustion Science and Technology*, vol. 185, article 4, pp. 676–709, 2013.

[44] C. Meneveau and T. Poinsot, "Stretching and quenching of flamelets in premixed turbulent combustion," *Combustion and Flame*, vol. 86, no. 4, pp. 311–332, 1991.

[45] H. Tennekes and J. L. Lumley, *A First Course in Turbulence*, MIT press, Cambridge, Mass, USA, 1972.

[46] K. R. Sreenivasan and R. A. Antonia, "The phenomenology of small-scale turbulence," *Annual Review of Fluid Mechanics*, vol. 29, pp. 435–472, 1997.

[47] R. A. Antonia and K. R. Sreenivasan, "Log-normality of temperature dissipation in a turbulent boundary layer," *Physics of Fluids*, vol. 20, no. 11, pp. 1800–1804, 1977.

[48] J. Mi, R. A. Antonia, and F. Anselmet, "Joint statistics between temperature and its dissipation rate components in a round jet," *Physics of Fluids*, vol. 7, no. 7, pp. 1665–1673, 1995.

[49] L. K. Su and N. T. Clemens, "The structure of fine-scale scalar mixing in gas-phase planar turbulent jets," *Journal of Fluid Mechanics*, no. 488, pp. 1–29, 2003.

[50] A. N. Karpetis and R. S. Barlow, "Measurements of scalar dissipation in a turbulent piloted methane/air jet flame," *Proceedings of the Combustion Institute*, vol. 29, no. 2, pp. 1929–1936, 2002.

[51] D. Geyer, A. Kempf, A. Dreizler, and J. Janicka, "Scalar dissipation rates in isothermal and reactive turbulent opposed-jets: 1-D Raman/Rayleigh experiments supported by LES," *Proceedings of the Combustion Institute*, vol. 30, no. 1, pp. 681–689, 2005.

[52] C. N. Markides and E. Mastorakos, "Measurements of scalar dissipation in a turbulent plume with planar laser-induced fluorescence of acetone," *Chemical Engineering Science*, vol. 61, no. 9, pp. 2835–2842, 2006.

[53] W. P. Jones and P. Musonge, "Closure of the Reynolds stress and scalar flux equations," *Physics of Fluids*, vol. 31, no. 12, pp. 3589–3604, 1988.

[54] P. K. Yeung, S. S. Girimaji, and S. B. Pope, "Straining and scalar dissipation on material surfaces in turbulence: Implications for flamelets," *Combustion and Flame*, vol. 79, no. 3-4, pp. 340–365, 1990.

[55] E. Hawkes, R. R. Sankaran, J. C. Sutherland, and J. H. Chen, "Scalar mixing in direct numerical simulations of temporally evolving plane jet flames with skeletal CO/H_2 kinetics," *Proceedings of the Combustion Institute*, vol. 31, no. 1, pp. 1633–1640, 2007.

[56] N. Swaminathan and R. W. Bilger, "Scalar dissipation, diffusion and dilatation in turbulent H2-air premixed flames with complex chemistry," *Combustion Theory and Modelling*, vol. 5, no. 3, pp. 429–446, 2001.

[57] N. Chakraborty, M. Klein, and R. S. Cant, "Effects of turbulent reynolds number on the displacement speed statistics in the thin reaction zones regime of turbulent premixed combustion," *Journal of Combustion*, vol. 2011, Article ID 473679, 19 pages, 2011.

[58] G. Hartung, J. Hult, C. F. Kaminski, J. W. Rogerson, and N. Swaminathan, "Effect of heat release on turbulence and scalar-turbulence interaction in premixed combustion," *Physics of Fluids*, vol. 20, no. 3, Article ID 035110, 2008.

[59] K. W. Jenkins, M. Klein, N. Chakraborty, and R. S. Cant, "Effects of strain rate and curvature on the propagation of a spherical flame kernel in the thin-reaction-zones regime," *Combustion and Flame*, vol. 145, no. 1-2, pp. 415–434, 2006.

[60] M. Klein, N. Chakraborty, K. W. Jenkins, and R. S. Cant, "Effects of initial radius on the propagation of premixed flame kernels in a turbulent environment," *Physics of Fluids*, vol. 18, no. 5, Article ID 055102, 2006.